Annals of Operations Research
https://doi.org/10.1007/s10479-025-06904-1

ORIGINAL RESEARCH

A metaheuristic approach for the multi-objective sustainable vehicle routing problem

Reza Moghdani[1,2] · Khodakaram Salimifard[1] · Emrah Demir[3] · Sasan Barak[2,4] · Adel Aazami[5] · Seyed Ashkan Hosseini Shekarabi[6]

Received: 26 December 2024 / Accepted: 13 October 2025

Abstract
This study introduces the Multi-Objective Sustainable Vehicle Routing Problem (MOSVRP) with time windows, designed for congested urban networks. The model simultaneously addresses economic, environmental, and social sustainability by minimizing costs and emissions while maximizing customer satisfaction through enhanced service at pickup nodes. To manage the complexity of large-scale urban routing, we propose a novel Voronoi diagram-based network shrinking procedure that significantly reduces computational effort. More specifically, the model incorporates time-dependent traffic patterns to capture realistic urban conditions. For the solution, we propose a tailored metaheuristic, the enhanced Multi-Objective Volleyball Premier League (MOVPL) algorithm, which incorporates reference point guidance, disruption operators, and adaptive weight adjustment. This hybrid approach effectively balances conflicting objectives and improves solution diversity. Applied to Tehran's urban freight network, the proposed method demonstrates superior performance across all metrics compared to benchmark algorithms and exact methods. Results show notable reductions in fuel consumption and travel distance, alongside improved service equity. Furthermore, the framework offers a scalable and transferable solution for sustainable logistics in other urban contexts.

Keywords Vehicle routing problem · Sustainability · Voronoi diagram · Multi-objective volleyball premier league algorithm

1 Introduction

During the last decade, high population growth in developing cities has become a significant challenge for the sustainable development of countries. Approximately 60% of the world's population currently lives in urban areas. This phenomenon is more intensified in some countries; for example, 75.4% of Iran's population lives in congested urban areas (Worldbank, 2018). From an urban planning perspective, traffic congestion is considered a primary concern for both commuters and logistics companies. Due to the high level of congestion, greenhouse gas (GHG) emissions generated by transportation have increased more

Extended author information available on the last page of the article

in absolute terms than any other industry. To address these concerns, cutting-edge solutions based on artificial intelligence (AI) have emerged, using predictive analytics and real-time data to reduce the impacts of congestion on urban networks. Recent studies have integrated metaheuristic algorithms with AI to address Vehicle Routing Problems (VRPs) considering environmental factors (see, e.g., Goli et al. (2018); Elshaer & Awad, 2020; Konstantakopoulos et al., 2022; Ma et al., 2025; Priyadarshi, 2024).

Sustainability is among the most critical issues facing contemporary society across a spectrum of economic, social, and environmental factors (Pilati & Tronconi, 2024). Most real-world routing applications include one or two of these factors in their proposed models. Therefore, consideration of all dimensions of sustainability can provide better solutions to the current challenges of most businesses (Garside et al., 2024), especially when integrated with AI approaches for an informed decision-making (Stamadianos et al., 2024; Tarhini et al., 2022). Figure 1 depicts the relationship between the three pillars of sustainability. According to this figure, if these concepts are implemented, the system may be equitable (social and economic), viable (environmental and economic), and bearable (social and environmental) (Vega-Mejía et al., 2019). In respect of this elegant framework, factoring social fairness, economic profitability, and environmental greenery into the practice is delusive. Therefore, we propose a novel mathematical model to support sustainable decisions in logistics systems.

At the operational level, the VRP has been widely studied in the literature (Dantzig & Ramser, 1959). In the standard VRP model, it is generally assumed that the arcs connecting nodes are based on fixed parameters, such as traveling time or distance. However, the cost function of any proposed VRP and its variants strictly depends on the quality of obtained routes, inherently related to the type of urban network representation. When time is considered the main factor in network representation, new variants of VRP emerge in the operations research literature (see, e.g., Moghdani et al. (2021); Lin et al. (2014); Zhang et al., (2022); Ghosh and Roy, (2023). We present a new approach to selecting the best path in the road transportation network for the studied VRP that minimizes three different objectives. To reach the best trade-off among these objectives, we consider multiple paths for any arc connecting two nodes in a graph and different levels of traffic congestion. Many paths con-

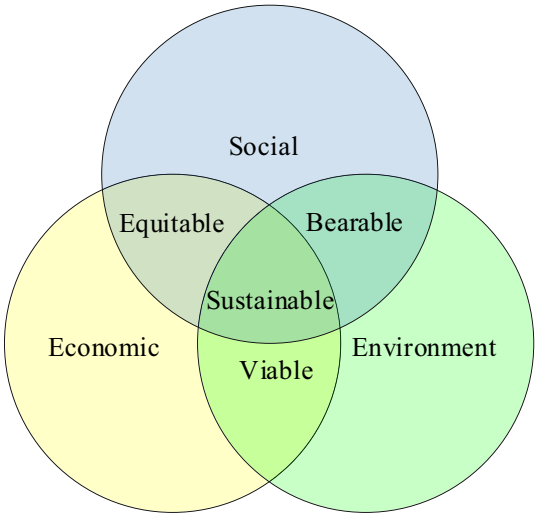

Fig. 1 The three pillars of sustainability (Source: Purvis et al., 2019)

nect two nodes in the urban network, and we deliberately discard many such non-promising paths by using an innovative procedure. Hence, the studied problem is termed multi-objective sustainability VRP (MOSVRP). Our proposed model embraces the capabilities of AI to manage computational complexity and effectively adapt to dynamic traffic conditions.

Most freight transportation companies that incorporate pick-up/delivery services are tremendously attempting to enhance customer satisfaction through on-time deliveries and low cost. In the basic version of VRPs (i.e., VRPTW, CVRP), servicing all customers in specified time windows is a straightforward task. In contrast, regarding VRP with pick-up and delivery (VRPPD), logistics service providers (LSPs) prioritize responding to the delivery nodes first and then trying to satisfy pick-up nodes. Therefore, in many real-world applications, it can be said that the number of pick-up nodes covered by distributors can be postulated as a sign of customer satisfaction.

High-resolution traffic telemetry, now routinely collected from connected fleets, has revealed nonlinear energy penalties associated with micro-scale stop-and-go patterns (Grote et al., 2016; X. Zhang et al., 2024a, 2024b). Recent path-generation studies calibrate battery-discharge curves against these data and demonstrate that modest speed moderation on congestion-prone arcs can defer recharging events without affecting schedule (Jeong et al., 2024; Lee et al., 2022). Building on this insight, adaptive departure-time rules coupled with flexible cruising-velocity choices have produced double-digit reductions in total energy use for city-centre parcel operations (Jeong et al., 2024; Woo et al., 2024). Advances in social sustainability put equity as a primary design objective (Eltoukhy et al., 2025). Integrating straightforward fairness measures into the routing objective spreads waiting times more evenly across customers without noticeably increasing the vehicle routes (Aleksandrov, 2025; Yu et al., 2024). Similar gains emerge when workload-regularity constraints are imposed on driver schedules, confirming that balanced service patterns and operational efficiency need not be mutually exclusive (Nekooghadirli et al., 2025). Coordinating trucks and drones so that they meet at well-timed meeting points and perform rapid battery swaps can shorten delivery in urban areas while cutting fuel use and emissions (Cui et al., 2024).

Other research shows that on-route energy sharing among electric vans can help charging-station demand peaks, smoothing network-wide power loads by up to twenty percent (Emami & Ramezani, 2024). Despite this momentum, three critical challenges still exist. First, most multi-objective formulations still lower pick-up coverage to a soft penalty rather than a headline criterion (Comert & Yazgan, 2023). Second, the combinatorial growth caused by congestion-aware multi-path structures challenges conventional neighbourhood searches (Hu et al., 2022). Third, cooperative energy-exchange protocols remain largely separated from routing decisions (J. Zhang et al., 2024a, 2024b). The MOSVRP addresses these gaps through a dominance-based path-pruning routine and an adaptive volleyball-league metaheuristic enriched with disruption moves and self-tuning reference points, thereby aligning cost efficiency, emission mitigation, and inclusive service within a single decision-support framework. The main contributions of this paper are as follows:

(i) A MOSVRP with time windows is proposed for congested urban road networks.
(ii) We design and apply a new heuristic algorithm based on the Voronoi diagram method to reduce network size, in which all redundant paths are discarded from the network based on emissions.

(iii) We incorporate time-dependent modeling of traffic congestion to ensure realistic route planning under varying travel speeds.
(iv) We enhance an existing multi-objective volleyball premier league approach with disruption operators, adaptive weight adjustments, and reference point guidance, thus effectively balancing cost minimization, emission reduction, and social satisfaction in large-scale urban logistics.

The content of this paper is organized as follows. In the second section, we provide a comprehensive literature review to identify the possible gaps that justify the existence of current work. We describe our proposed mathematical model in Sect. 3. In Sect. 4, the main approaches used in this study are presented, and the numerical experiment is shown in Sect. 5, as well as a sensitivity analysis on several parameters. Finally, we provide conclusions and future research directions in Sect. 6.

2 Literature review

Numerous attributes commonly faced in real-world urban freight transportation settings have been considered in this paper; for example, time-varying road congestion, multipath selection, sustainable VRP (SVRP), and time-dependent VRP (TDVRP). Interested readers can refer to Demir et al. (2014b) for CO_2 emissions calculation methods, Gendreau et al. (2015) for the TDVRP studies, and Ben Ticha et al. (2018) for a review of the urban network on VRPs.

2.1 Sustainability in road freight transportation

All three pillars of sustainability have rarely been covered in the context of green logistics. Most studies examined only environmental and economic insights, while very few addressed social issues. By reviewing the most relevant papers in this field, it is apparent that the social sustainability concept has explored issues such as human resources, safety concerns, and customer satisfaction. Ramos and Oliveira (2011) aimed to minimize balancing the workload as an essential social concern among stops using a heuristic model. Labuschagne et al. (2005) placed social concerns in the human resources category by recognizing that equity and safety issues are regarded as social concerns included within the internal human resources category.

Once the role of the human factor emerges in the routing problem, the vital issue of safety arises. Surprisingly, little attention has been paid to possible traffic accidents and environmental concerns. The most relevant study, conducted by Li et al. (2019), developed a multi-depot GVRP regarding four objectives, including revenues, cost, time, and emissions, by using an improved ant colony optimization algorithm. Moutaoukil et al. (2014) stated that social indicators (e.g., accident risk, noise, and congestion) are challenging to measure, and they considered the number of vehicles and total traveling distance. Li et al. (2008) studied a significant aspect of social sustainability regarding balancing the routes assigned to various stops, wherein the workload of people was considered to receive more equity in this case. Therefore, the primary objective is to minimize the differences between the longest route and the shortest route lengths. This problem, termed VRP with route balancing (VRPRB),

was recently addressed by several researchers (Jozefowiez et al., 2009; Lacomme et al., 2015). A stochastic variant of VRP with multiple objectives in a green context is studied by (Elgharably et al., 2022). The authors investigated three different objectives, namely, economic, environmental, and social aspects (i.e., customer satisfaction). A novel hybrid heuristic algorithm is proposed to solve the proposed mathematical model. Li et al. (2021) presented a mathematical model for the multi-depot VRP considering limited resources to maximize customer satisfaction. An improved variable neighborhood algorithm is proposed for the mixed-integer mathematical model with a nonlinear objective function to solve the problem. Besides, an improved K-means algorithm and an adaptive mechanism are added to generate the initial solution and the solution procedure. A multi-commodity flow optimization model is proposed by (Wang et al., 2022) for food distribution services with timeliness requirements, vehicle capacity, and mixed-loading strategy. An improved Lagrangian Relaxation method is used to decompose and solve the problem with a dynamic programming algorithm using an alternating direction method of multipliers (ADMM)-based solution framework.

Ibarra-Rojas and Silva-Soto (2021) investigated a mixed-integer linear programming (MILP) model to address an egalitarian distribution system to maximize the minimum fraction of fulfilled demand and minimize delivery times. A commercial solver and a genetic algorithm provide the exact and approximate solutions. Salehian et al. (2019) presented a VRP to reduce fuel consumption and maximize customer satisfaction. A metaheuristic method based on the bee algorithm (BA) is proposed to solve the problem on a large scale. Qin et al. (2019) studied the impact of carbon price on carbon emissions and customer satisfaction by proposing a mathematical model for a cold chain VRP to minimize the cost of satisfying a unit of customers. Moreover, a cycle Evolutionary Genetic Algorithm is suggested to solve the problem. Zhang et al. (2018) addressed the CGVRP for alternative fuel vehicles with fuel and load limitations, proposing heuristic and Ant Colony System algorithms. Their methods were validated via comprehensive simulations, showing robust performance. Rojas-Saavedra et al. (2023) developed a hybrid metaheuristic integrating Variable Neighborhood Search and GRASP for the 3L-FHFVRP, achieving superior results and promoting sustainable transportation solutions.

Goodarzi et al. (2024) developed a two-stage stochastic optimization model that integrates consolidation into intermodal freight routing to improve both sustainability and resilience. The model captures economic, environmental, and social impacts, including GHG emissions, noise, congestion, and accidents, while allowing decision-makers to select both proactive preparedness and reactive recovery strategies. Solved with a Lagrangian relaxation scheme on United Kingdom data, the approach shows that spending only 0.4 percent of the total cost on resilience can cut overall expenses by roughly 4.7 percent. Rahiminia et al. (2025) introduced a P-robust, chance-constrained rail–road network model that trims worst-case cost regret by about 24 percent while adding only 1.4 percent to expected expenditure, making freight flows both greener and more disruption-proof.

2.2 Time-dependent VRP

In examining traffic congestion in routing problems, Malandraki and Daskin (1992) initially formulated TDVRP, after which Malandraki and Dial (1996) proposed a dynamic programming approach to solve similar problems. The main shortcoming of these studies related to

neglecting the FIFO property, which was later embedded in TDVRP by Ichoua et al., (2003) and Fleischmann et al., (2004).

Solving the time-dependent shortest path problem (TDSPP) is the primary objective of coping with traffic congestion in TDVRPs. Eglese et al. (2006) attempted to apply this approach to a real-world problem in the UK. Later, Kok et al. (2012) used dynamic extension programming to employ TDSPP on TDVRP. We note that implementing TDVRP based on emission path requires both departure time and vehicle load for all arcs, which indicates that TDVRP is more complicated than TDSPP. In recent studies, several authors (see, e.g., Ehmke et al., 2016a; Qian & Eglese, 2014)) applied emission models. Later, Ehmke et al. (2016b) implemented a straightforward method that computed emission-minimizing paths independent of vehicle payload. They used a Tabu search (TS) on an entire urban network to obtain an optimal path for considering TDVRP. Combined with an exact approach named column generation, Qian and Eglese (2016) implemented the TS method to determine optimal paths. Verbeeck et al. (2017) designed a rapid Ant Colony System to tackle the time-dependent orienteering problem with time windows (TD-OPTW), addressing time-dependent disruptions with real-world benchmarks. Their solution achieved exceptional performance in practical routing scenarios. Rastani and Çatay (2023) extended the electric vehicle routing problem with time windows (LD-EVRPTW) by including load-dependent energy consumption, proposing a Large Neighborhood Search-based matheuristic with an optimal repair mechanism. Their results highlighted significant changes in route planning and costs due to load variations. Li (2024) introduced a dual-objective model for fresh product logistics, balancing customer satisfaction, cost, and carbon emissions using a Multi-objective Artificial Bee Colony algorithm. The study effectively demonstrated cost savings and emission reductions through Pareto analysis. Eltoukhy et al. (2025) introduced the multi-trip time-dependent VRPTW, uncertain unloading time, and environmental and social considerations, and tackled it with a neural-network-guided mixed-integer model and an ant colony optimization algorithm. Applied to Hong Kong modular integrated construction, the solution satisfied every delivery, eliminated all GHG cap breaches. It revealed that omitting social impacts can hide about forty percent of true costs, while the sustainable plan increases expected spending by only 1.5 percent.

2.3 Green VRP

The term *green* was first used by Erdoğan and Miller-Hooks (2012) in the context of freight transportation problems, which focused on Alternative Fuel stations (AFS) with a limited capacity of vehicles and constrained refueling infrastructure. In the same vein, Bruglieri et al. (2016) attempted to propose a more realistic model of GVRP through a new formulation investigating the reduction in the number of AFSs. Other studies in the area of GVRP were conducted by Kopfer and Kopfer (2013) and Kwon et al. (2013) on the heterogeneous fleet of vehicles.

One of the most important variations of GVRP is the Pollution-Routing Problem (PRP), proposed by Bektaş and Laporte (2011). They used the Comprehensive Modal Emission Model (CMEM) to measure fuel consumption in their proposed model. Demir et al. (2012) used a metaheuristic algorithm, Adaptive Large Neighborhood Search (ALNS), to solve the PRP. Later, Demir et al. (2014a) proposed a bi-objective PRP minimizing both functions, including fuel driving time and fuel consumption. In another study, Tajik et al. (2014)

appraised the PRP with pickups and deliveries, and performed a new robust approach to cope with this problem. Dabia et al. (2017) presented an identical approach based on a branch-and-price algorithm to solve the PRP problem. Furthermore, Raeesi and Zografos (2019) proposed Steiner PRP, as a new variant of this approach, on freight transportation urban networks by applying a precomputation procedure embedded in the path selection method, termed the path elimination procedure, to obtain an optimal path regarding the emissions minimization problem. Fernández Gil et al. (2023) developed a mathematical formulation addressing the cumulative vehicle routing problem with Time windows (CumVRP-TW), focusing on reducing fuel consumption and emissions. They employed a hybrid method combining GRASP with exact optimization, which showed promising results on standard benchmarks. Ferreira et al. (2024) proposed a variable-neighborhood-search metaheuristic for the GVRP with two-dimensional loading and split deliveries, a variant that minimizes GHG emissions while respecting packing and unloading rules. Their algorithm found 21 of 60 optimal solutions and improved the best found solution for 50 of 180 benchmark instances of the related capacitated variant, all within reasonable runtimes. Wang et al. (2025) defined the Dynamic time-dependent GVRP for decoration waste collection (DTDGVRP-DWC) and solved it with a two-stage scheme that marries competitive simulated annealing for the look-ahead schedule with an event-triggered real-time re-planner. The Beijing case study shows that once demand-prediction accuracy passes a modest threshold, this proactive, carbon-aware approach consistently outperforms reactive routing in both cost and emissions.

3 Research Gap

This section provides a summary of the most relevant works as listed in Table 1. We present various attributes of such studies and compare them with the current study.

Table 1 indicates four gaps that the current study aims to address: (*i*) although there are several attempts to propose an efficient algorithm that tackles the urban network into energy-minimization VRP, there is no efficient algorithm designed for large-scale problems in this domain; (*ii*) limited research examines all pillars of sustainability with their mathematical models; (*iii*) only two studies propose multi-objective optimization incorporating their mathematical model; (*iv*) the general framework only integrates some attributes presented in this table; (*v*) no significant study incorporates time-dependency approach into GVRPs mathematical model regarding all aspects of sustainability; (*vi*) the maximum number of pickup node has been considered as a social factor in this study.

Despite these insights, the literature still lacks a solution that meets three objectives at the same time. First, no published study models a large city network with time-varying congestion while allowing several alternative paths between each pair of nodes. Second, existing formulations seldom treat cost, GHG emissions, and customer coverage as goals of equal importance, which limits their value for balanced policy making. Third, the few methods that do examine energy use or social service levels usually ignore traffic dynamics or remain limited to small benchmark instances. To fill these gaps, the present work introduces a MOSVRP that combines time-varying speeds, multi-path routing, and the three pillars of sustainability in a single framework. The model is solved with a dominance-driven path reduction procedure followed by an adaptive volleyball league metaheuristics that scales to

Table 1 A review of the most related studies with different attributes

Reference	Obj	T-D	Mp	Solution methodology			Cs/Ti/Cct	The three pillars of sustainability		
				Ex/Met	HeV	OID		Eco	Env	Soc
Li et al. (2008)	So	×	×	Met	×	×	Cs	√	×	√
Kuo (2010)	So	√	×	Met	×	×	Ti	√	√	×
Maden et al. (2010)	So	√	×	Met	√	×	Ti	√	√	×
Bektaş and Laporte (2011)	So	×	×	Ex	×	×	Ti	√	√	×
Ramos and Oliveira (2011)	So	×	×	Met	×	×	Cs	√	×	√
Figliozzi (2011)	Bo	√	×	Met	×	×	Cs	√	√	×
Jabali et al. (2012)	So	×	×	Met	×	×	Ti	√	√	×
Erdoğan and Miller-Hooks (2012)	So	×	×	Ex	×	×	Ti	√	√	×
Demir et al. (2012)	So	×	×	Met	√	×	Ti	√	√	×
Kok et al. (2012)	So	√	×	Met	×	×	Ti	√	×	×
Kopfer and Kopfer (2013)	So	×	×	Ex	×	×	Ti	√	√	×
Franceschetti et al. (2013)	So	√	×	Ex	×	×	Ti	√	√	×
Moutaoukil et al. (2014)	So	×	×	Ex	×	×	Cs	√	√	√
Demir et al. (2014a)	Bo	×	×	Met	√	×	Ti	√	√	×
Lacomme et al. (2015)	So	×	×	Met	√	×	Ti	√	×	√
Bruglieri et al. (2016)	So	×	×	Ex	×	×	Ti	√	√	×
Qian and Eglese (2016)	So	√	√	Met	√	×	Ti	√	√	×
Ehmke et al. (2016b)	So	√	√	Met	√	×	Ti	√	√	×
Raeesi and Zografos (2019)	Mo	√	√	Ex	×	×	Cct	√	√	×
Mancini (2017)	So	×	√	Met	√	×	Ti	√	√	×
Androutsopoulos and Zografos (2017)	Bo	×	√	Met	×	×	Ti	√	√	×
Huang et al. (2017)	Bo	×	√	Ex	×	×	Cs	√	√	×
Li et al. (2019)	Mo	×	×	Met	×	×	Ti	√	√	×
Salehian et al. (2019)	So	×	×	Ex/Met	×	×	Ti	√	×	√
Qin et al. (2019)	So	×	×	Ex/Met	×	×	Cct	×	√	√
Bruglieri et al. (2019)	So	×	×	Ex	×	×	Ti	√	√	×
Sonu Rajak et al. (2020)	So	×	×	Ex/Met	×	×	Ti	√	×	√
Li et al. (2021)	So	×	×	Met	×	×	Ti	×	×	√
Ibarra-Rojas and Silva-Soto (2021)	So	×	×	Ex/Met	×	×	Cct	√	×	√
Elgharably et al. (2022)	Mo	×	×	Met	√	×	Ti	√	√	√
Wang et al. (2022)	So	×	×	Ex	×	×	Ti	√	×	√
Revanna and Al-Nakash (2023)	So	×	×	Met	√	×	Ti	√	√	√
Xiao et al. (2024)	So	×	×	Ex/Met	×	×	Ti	√	√	×
Li (2024)	Mo	×	×	Met	×	×	Ti	√	√	√
This study	Mo	√	√	Met	√	√	Cct	√	√	√

Abbreviations: Obj: objective function, (T-D): Time-Dependency So: single objective, Bo: bi-objective, Mo: many-objective, Mp: multiple paths, Ex: exact approach, Met: metaheuristic approach, HeV: heuristic of VRPs, Cs: case study, Ti: test instance, Cct: a combination of the case study and test instance, Eco: economic, Env: environmental, Soc: social

real megacity data. This integrated design directly responds to the shortcomings identified above and provides a more comprehensive decision support approach for researchers and practitioners.

4 Model setting

4.1 Problem description

Tehran, Iran, one of the most populous cities in the Middle East, experiences intense traffic congestion and heightened environmental challenges. Coupled with a significant proportion of Iran's rapidly growing urban population now residing in Tehran, local logistics service providers face a pressing need to optimize last-mile freight deliveries. Given such constraints, reducing operational costs, mitigating the environmental impacts of carbon emissions, and maintaining high customer satisfaction are critical. These three economic, environmental, and social factors are often referred to as the pillars of sustainability and collectively define the necessity for a more holistic perspective in vehicle routing. Traditional VRPs insufficiently address social factors like equitable or enhanced service for pickup customers, especially in congested networks like Tehran. Hence, formulating a multi-objective model that simultaneously caters to cost minimization, emission reduction, and improved customer satisfaction holds tremendous potential in advancing sustainable urban freight operations across Iran.

MOSVRP presented in this paper accommodates time-window constraints, variable traffic congestion, and the simultaneous pickup and delivery of goods. It integrates an innovative Voronoi diagram-based network shrinking procedure to manage Tehran's large-scale road network, thereby increasing solvability and computational efficiency. Furthermore, it adopts an enhanced metaheuristic, building on the multi-objective volleyball premier league algorithm, that leverages a reference point strategy, disruption operator, and adaptive weight adjustment. This comprehensive methodology not only optimizes routes for lowered costs and carbon emissions but also emphasizes serving the maximum number of pickup nodes. The proposed approach provides evidence of its viability by situating the study in Tehran. It offers decision-makers a powerful tool for orchestrating socially responsible, economically feasible, and ecologically sound urban freight distribution. It is worth mentioning that the developed model and solution approach will definitely be applicable and implementable for other similar cities around the globe. The following section provides an overview of the notations used in this study and a general description of the proposed model.

5 Notations and model formulation

In this sub-section, we provide Table 2 to present the list of notations used in this paper.

In this study, we use two different layers, including geographical and customer graphs, to construct the customer's location and urban network. An illustration appears in Fig. 2.

A typical customer graph, the first layer, is defined as $\mathcal{G}^c = (\mathcal{N}^c, \mathcal{A}^c)$, in which set $\mathcal{N}^c = 0 \cup \mathcal{N}^+ \cup \mathcal{N}^-$ symbolizes the depot $i \in \mathcal{N}^c = \{0\}$, customer locations of pick-up $\mathcal{N}^+$, customer locations of delivery $\mathcal{N}^-$. Each customer i is defined with a hard time win-

Table 2 The list of notations used in this study

Notation	Description
$\mathcal{G}^c$	Customer graph
$\mathcal{N}^c$	Set of customer nodes
$\mathcal{A}^c$	Set of arcs connecting pairs of customer nodes
$\mathcal{N}^+$	Pickup nodes
$\mathcal{N}^-$	Delivery nodes
$\mathcal{G}^G$	Geographical graph
$\mathcal{A}^G$	Set of intersections
$\mathcal{N}^G$	Set of road segments
$[\varepsilon, \mathcal{L}]$	the planning horizon
$\mathrm{P_{ij}}$	Set of paths connecting arc $(i,j) \in \mathcal{N}^C$
$\wp_{ij}^P$	A path in the set P_{ij}
q_i	The demand for customer node $i \in \mathcal{N}^C \setminus \{0\}$
s_i	Service time of customer node $i \in \mathcal{N}^C \setminus \{0\}$
K	Set of homogenous vehicle $K = \{1, 2, .., k\}$
Q	The capacity of a vehicle
R	Number of periods with constant speed
ψ_e, ψ_s, ψ_w	Coefficients in CMEM model to calculate fuel consumption
μ	Vehicle curb-weight
$F(v,t,f)$	Fuel consumption function of constant speed v, duration t, and vehicle load f
v_{ij}^{pr}	Speed in period r on path $\wp_{ij}^P$
w	Departure time from a node
$\tau_{ij}^p(w)$	Piecewise linear travel time function of departure time w from node i on path $\wp_{ij}^P$
M_{ij}^p	Intervals of the piecewise linear travel time function $\tau_{ij}^p(w)$ on path $\wp_{ij}^P$
$\left[b_{ij}^{pm}, b_{ij}^{p,m+1}\right]$	m th interval of travel time function $\tau_{ij}^p(w)$ on path $\wp_{ij}^P$
t_{ij}^{pr}	Travel time at the speed v_{ij}^{pr} if the vehicles depart from node at time b_{ij}^{pm} on path $\wp_{ij}^P$
$\tau_{ij}^{pr}(w)$	Piecewise linear travel time function of departure time w at speed v_{ij}^{pr} on path $\wp_{ij}^P$
θ_{ij}^{pmr}	The slope of the piecewise linear function $\tau_{ij}^{pr}(w)$ within interval $\left[b_{ij}^{pm}, b_{ij}^{p,m+1}\right]$ on path $\wp_{ij}^P$
η_{ij}^{pmr}	The intercept of the piecewise linear function $\tau_{ij}^{pr}(w)$ within interval $\left[b_{ij}^{pm}, b_{ij}^{p,m+1}\right]$ on path $\wp_{ij}^P$
d_{ij}^p	Distance of path $\wp_{ij}^P$
f_{ij}^p	Vehicle load carried on the path $\wp_{ij}^P$
$F_{ij}^p(w)$	Fuel consumption of departure time w from node on path $\wp_{ij}^P$
S	Number of discretized time points to calculate the time-dependent shortest path
x_{ij}	Equal to 1 if arc (i,j) is on the optimal route
x_{ij}^p	Equal to 1 if the vehicle travels on the path $\wp_{ij}^P$
	Eal to 1 if the departure time at node toward node j is in $\left[b_{ij}^{pm}, b_{ij}^{p,m+1}\right]$
x_{ij}^k	Equal to 1 if the vehicle k travels on the arc (i,j)
f_{ij}	The load carried on arc (i,j)
ϑ_{ij}^{pm}	Earliest possible departure time at node on path $\wp_{ij}^P$
w_{ij}^{pm}	al departure time at node (in $\left[b_{ij}^{pm}, b_{ij}^{p,m+1}\right]$) on path $\wp_{ij}^P$
$\left[\overline{e}_i, \overline{\ell}_i\right]$	Hard time windows of customer node $i \in \mathcal{N}^C \setminus \{0\}$

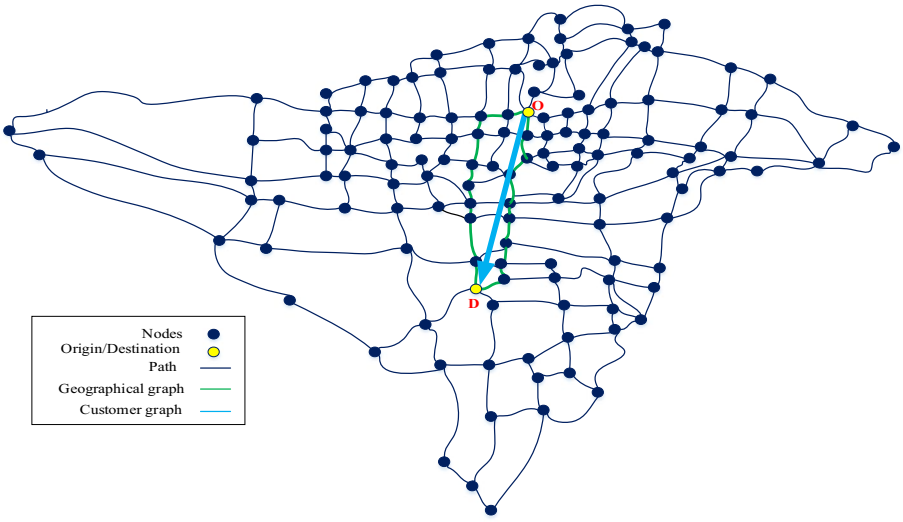

Fig. 2 A typical representation of the geographical and customer graph of Tehran city

dow $\left[\overline{e}_i, \overline{\ell}_i\right]$, service time s_i and demand q_i. Finally, set $\mathcal{A}^c$ represents the arcs connecting all node pairs. The homogeneous fleet has K vehicles, each with a capacity Q. Vehicles should serve all customers within the delivery time horizon, which is defined as $[\varepsilon, \mathcal{L}]$.

The second layer of the proposed network shows the actual road network, known as the geographical graph $\mathcal{G}^g = (\mathcal{N}^g, \mathcal{A}^g)$. $\mathcal{N}^g$ signifies the set of connections and $\mathcal{A}^g$ symbolizes the set of road segments in the road network. Each connection between two customers $(i, j) \in \mathcal{A}^c$ can represent a set of paths in the geographical graph. Let P_{ij} denote a set of multipaths for an arc $(i, j) \in \mathcal{A}^c$, which can be defined as $P_{ij} = \left\{\wp_{ij}^1, \wp_{ij}^2, \ldots, \wp_{ij}^{|P_{ij}|}\right\}$. Each member of P_{ij} connects nodes i and j in $\mathcal{N}^g$, and $\wp_{ij}^p = \left\{a_1^p, a_2^p, \ldots, a_{|\wp_{ij}^p|}^p\right\}$ is defined as a finite sequence of road segments in $\mathcal{A}^g$.

5.1 Preliminaries

The basic assumptions of the proposed model, including fuel consumption and the time-dependent travel time functions, are presented here.

5.1.1 Fuel consumption

There is a rich literature using the CMEM (Bektaş & Laporte, 2011; Demir et al., 2012). This model, introduced by (Barth & Boriboonsomsin, 2009) to measure the amount of CO_2 emissions, is considered the first objective of this paper, connecting to environmental concerns. Let d be the distance between two nodes and t travel time with constant speed v and the vehicle carries a load f; therefore, the fuel consumption $F(t, v, f)$ can be formulated as:

$$F(t, v, f) = \psi_e t + \psi_s v^3 t + \psi_w d(\mu + f), \tag{1}$$

where ψ_e, ψ_s, and ψ_w denote the coefficients used in this formula for engine, speed, and weight modules, respectively, and μ denotes vehicle curb-weight. A detailed description of the CMEM model is presented in Appendix A.

5.1.2 Time-dependent travel time model

To obtain the travel time model, R periods are considered in the delivery time horizon $[\varepsilon, \mathcal{L}]$ and a vehicle has a constant speed v at each road segment within a period$r$. A step function is defined to determine the travel speed at the road segment. Several approaches could estimate travel speed, and one of the most practical is a piecewise linear function presented by (Ichoua et al., 2003). In our study, the same procedure, using a piecewise linear function for the conversion, is implemented. In the typical path $\wp_{ij}^P$, travel time function $\tau_{ij}^p(.)$ is used. Like other studies in the literature (e.g.,(Donati et al., 2008), we have applied the same procedure using the travel time function $\tau_{ij}^p(.)$.

Considering the piecewise linear travel time function $\tau_{ij}^p(.)$ of path $\wp_{ij}^P$, a set of breakpoints, $\mathrm{b} = \left[b_{ij}^{pm}, b_{ij}^{p,m+1}\right]$, where $m = 1, .., M_{ij}^P$, is defined to compute the travel time of arc (i, j). It is worth mentioning here that the first and last members (b_{ij}^{p1} and b_{ij}^{p,M_{ij}^p+1}) of a finite set are equal to the boundary of the delivery time horizon ($b_{ij}^{p1} = \varepsilon$ and $b_{ij}^{p,M_{ij}^p+1} = \mathcal{L}$).

Let $w \in \left[b_{ij}^{pm}, b_{ij}^{p,m+1}\right]$ denotes departure time from node i to node j with travel time t_{ij}^{pmr} at speed v_{ij}^{pr} traversing the path $\wp_{ij}^P$, travel time of the corresponding path is calculated as:

$$\tau_{ij}^{pr}(\mathrm{w}) = \frac{t_{ij}^{p,m+1,r} - t_{ij}^{pmr}}{b_{ij}^{p,m+1} - b_{ij}^{pm}}\left(w - b_{ij}^{pm}\right) + t_{ij}^{pmr}. \tag{2}$$

Hence, the linear travel time formula $\tau_{ij}^p(.)$ is a function of departure time w, the slope and interception can be calculated as:

$$\theta_{ij}^{pm} = \frac{t_{ij}^{p,m+1,r} - t_{ij}^{pmr}}{b_{ij}^{p,m+1} - b_{ij}^{pm}}, \tag{3}$$

$$\eta_{ij}^{pmr} = t_{ij}^{pmr} - b_{ij}^{pm}\frac{t_{ij}^{p,m+1,r} - t_{ij}^{pmr}}{b_{ij}^{p,m+1} - b_{ij}^{pm}}, \tag{4}$$

where θ_{ij}^{pm} and η_{ij}^{pmr} denote slope and interception of travel time formula, respectively. Therefore, the following formula is obtained:

$$\tau_{ij}^{pr}(\mathrm{w}) = \theta_{ij}^{pmr} w + \eta_{ij}^{pmr}. \tag{5}$$

Finally, the total travel time of the path $\wp_{ij}^P$ can be computed as:

$$\begin{aligned}\tau_{ij}^{p}(\mathrm{w}) &= \sum_{r=1}^{R} \tau_{ij}^{pr}(\mathrm{w}) \\ &= \sum_{r=1}^{R} \theta_{ij}^{pmr} w + \sum_{r=1}^{R} \eta_{ij}^{pmr}.\end{aligned} \tag{6}$$

We can simply use travel time function $\tau_{ij}^{p}(\mathrm{w})$ instead of time t in fuel consumption formula, and then hereafter, the fuel consumption of a vehicle travelling on a path $\wp_{ij}^{P}$ can be rewritten as:

$$\begin{aligned}F_{ij}^{p}(w) &= \psi_e \left[\sum_{r=1}^{R} \theta_{ij}^{pmr} w + \sum_{r=1}^{R} \eta_{ij}^{pmr}\right] \\ &+\psi_s \left[\sum_{r=1}^{R} \left(v_{ij}^{pr}\right)^3 \theta_{ij}^{pmr} w + \sum_{r=1}^{R} \left(v_{ij}^{pr}\right)^3 \eta_{ij}^{pmr}\right] \\ &+\psi_w d_{ij}^{p}\left(\mu + f_{ij}^{p}\right),\end{aligned} \tag{7}$$

where d_{ij}^{p} and f_{ij}^{p} denote the distance and load carried on path $\wp_{ij}^{P}$, respectively.

5.2 The time-dependent shortest path problem

We examine the linear travel time function for a link in which the shortest path from node i to node j is measured, based on the Dijkstra's algorithm. We note that the shortest path problem (SSP) has been proven to be an NP-hard problem (Dehne et al., 2012). In this study, we use the same procedure as used in Stølting Brodal and Jacob, (2004) to find an optimal path. For any link in this study, with predefined r discretised time points w. We calculate the shortest path for all points to create a set of unique time-dependent shortest paths. Therefore, generated paths comprise all possible routes between two connected nodes.

5.3 Mathematical model

In this section, we present a multi-objective mathematical model for a sustainable time-dependent vehicle routing problem, in which two significant operational decisions, including path selection and vehicle routing, are made to minimize three objectives simultaneously. Before presenting the mathematical model, the main assumptions related to this model are introduced as follows:

- All customers' demands must be satisfied within the specified (hard) time windows.
- The capacity of vehicles is limited.
- The time horizon for planning is limited.
- Between each pair of customers, there may be more than two feasible paths.
- A piecewise linear function has been regarded as a proposed time-dependent travel time model.
- A maximum number of pick-ups has been considered a social responsibility in this model.

We define the proposed mathematical model as follows:

$Minimise Z\left(z_1, z_2, -z_3\right)$, where:

$$
\begin{aligned}
z_1 = & \sum_{(i,j)\in\mathcal{A}^c} \sum_{m\in M} \sum_{p\in P} \psi_e \left[\sum_{r=1}^{R} \theta_{ij}^{pmr} w_{ij}^{pm} + \sum_{r=1}^{R} \eta_{ij}^{pmr} x_{ij}^{pm}\right] \\
& + \sum_{(i,j)\in\mathcal{A}^c} \sum_{m\in M} \sum_{p\in P} \psi_s \left[\sum_{r=1}^{R} \left(v_{ij}^{pr}\right)^3 \theta_{ij}^{pmr} w_{ij}^{pm} + \sum_{r=1}^{R} \left(v_{ij}^{pr}\right)^3 \eta_{ij}^{pmr}\right] \\
& + \sum_{(i,j)\in\mathcal{A}^c} \sum_{p\in P} \psi_w d_{ij}^{p} \left(\mu + f_{ij}^{p}\right)
\end{aligned} \tag{8}
$$

$$
z_2 = \sum_{(i,j)\in\mathcal{A}^c} \sum_{p\in P} d_{ij}^{p} x_{ij}^{p} \tag{9}
$$

$$
z_3 = \sum_{(i,j)\in\mathcal{N}^-} \sum_{k\in k} x_{ij}^{k} \tag{10}
$$

Subject to

$$
\sum_{j\in\mathcal{N}^c} x_{0j} \leq |K| \tag{11}
$$

$$
\sum_{i\in\mathcal{N}^-} x_{ij} = 1 \; \forall j \in \mathcal{N}^- \tag{12}
$$

$$
\sum_{j\in\mathcal{N}^-} x_{ij} = 1 \; \forall i \in \mathcal{N}^- \tag{13}
$$

$$
\sum_{i\in\mathcal{N}^+} x_{ij} \leq 1 \; \forall j \in \mathcal{N}^+ \tag{14}
$$

$$
\sum_{j\in\mathcal{N}^+} x_{ij} \leq 1 \; \forall i \in \mathcal{N}^+ \tag{15}
$$

$$
\sum_{j\in\mathcal{N}^+} x_{ij}^{k} + \sum_{j\in\mathcal{N}^-} x_{ij}^{k} \leq 1 \; \forall i \in \mathcal{N}^c \backslash \{0\}, \forall k \in K \tag{16}
$$

$$
\sum_{i\in\mathcal{N}^c} f_{ij} - \sum_{k\in\mathcal{N}^c} f_{jk} = q_j \; \forall j \in \mathcal{N}^c \backslash \{0\} \tag{17}
$$

$$
q_j x_{ij} \leq f_{ij} \leq \left(Q - q_i\right) x_{ij} \; \forall i, j \in \mathcal{N}^- \tag{18}
$$

$$q_i x_{ij} \leq f_{ij} \leq (Q - q_j)\, x_{ij}\ \forall i, j \in \mathcal{N}^+ \tag{19}$$

$$\sum_{p \in P} x_{ij}^p = x_{ij}\ \forall ij \in \mathcal{A}^c \tag{20}$$

$$\sum_{m \in M} x_{ij}^{pm} = x_{ij}^p\ \forall ij \in \mathcal{A}^c, \forall p \in P \tag{21}$$

$$\sum_{p \in P} f_{ij}^p = f_{ij}\ \forall ij \in \mathcal{A}^c \tag{22}$$

$$q_j x_{ij}^p \leq f_{ij}^p \leq (Q - q_i)\, x_{ij}^p\ \forall i, j \in \mathcal{N}^-, \forall p \in P \tag{23}$$

$$q_i x_{ij}^p \leq f_{ij}^p \leq (Q - q_j)\, x_{ij}^p\ \forall i, j \in \mathcal{N}^+, \forall p \in P \tag{24}$$

$$\vartheta_{0j}^{pm} = \varepsilon x_{0j}^{pm}\ \forall j \in \mathcal{N}^c \backslash \{0\}, \forall p \in P, \forall m \in M \tag{25}$$

$$\vartheta_{j0}^{pm} \leq \mathcal{L} x_{jo}^{pm}\ \forall j \in \mathcal{N}^c \backslash \{0\}, \forall p \in P, \forall m \in M \tag{26}$$

$$x_{ij}^{pm} b_{ij}^{pm} \leq w_{ij}^{pm} \leq x_{ij}^{pm} b_{ij}^{p,m+1}\ \forall ij \in \mathcal{A}^c, \forall p \in P, \forall m \in M \tag{27}$$

$$\begin{aligned} &\sum_{i \in \mathcal{N}^c} \sum_{p \in P} \sum_{m \in M} \left(\sum_{r=1}^{R} \theta_{ij}^{pmr} w_{ij}^{pm} + \sum_{r=1}^{R} \eta_{ij}^{pmr} x_{ij}^{pm} \right) + \sum_{i \in \mathcal{N}^c} \sum_{p \in P} \sum_{m \in M} w_{ij}^{pm} + S_j \\ &= \sum_{k \in \mathcal{N}^c} \sum_{p \in P} \sum_{m \in M} \vartheta_{jk}^{pm}\ \forall j \in \mathcal{N}^c \backslash \{0\} \end{aligned} \tag{28}$$

$$\begin{aligned} &\sum_{m \in M} \sum_{p \in P} \left(\sum_{r=1}^{R} \theta_{i0}^{pmr} w_{i0}^{pm} + \sum_{r=1}^{R} \eta_{i0}^{pmr} x_{i0}^{pm} \right) \\ &\leq \mathcal{L}\ \forall i \in \mathcal{N}^c \backslash \{0\} \end{aligned} \tag{29}$$

$$\begin{aligned} &x_{ij}^{pm} \bar{e}_i \leq \sum_{i \in \mathcal{N}^-} \sum_{p \in P} \sum_{m \in M} \left(\sum_{r=1}^{R} \theta_{ij}^{pmr} w_{ij}^{pm} + \sum_{r=1}^{R} \eta_{ij}^{pmr} x_{ij}^{pm} \right) \\ &\leq x_{ij}^{pm} \bar{\ell}_i\ \forall i \in \mathcal{N}^c \end{aligned} \tag{30}$$

$$x_{ij} \in \{0, 1\}\ \forall ij \in \mathcal{A}^c \tag{31}$$

$$x_{ij}^p \in \{0, 1\}\ \forall ij \in \mathcal{A}^c, \forall p \in P \tag{32}$$

$$x_{ij}^{pm} \in \{0, 1\}\ \forall ij \in \mathcal{A}^c, \forall p \in P, \forall m \in M \tag{33}$$

$$x_{ij}^k \in \{0, 1\}\ \forall ij \in \mathcal{A}^c, \forall k \in K \tag{34}$$

$$f_{ij} \geq 0 \; \forall ij \in \mathcal{A}^c \tag{35}$$

$$f_{ij}^{p} \geq 0 \; \forall ij \in \mathcal{A}^c, \forall p \in P \tag{36}$$

$$w_{ij}^{pm}, \vartheta_{ij}^{pm} \geq 0 \; \forall ij \in \mathcal{A}^c, \forall p \in P, \forall m \in M. \tag{37}$$

The first objective function, objective function (8), is used to minimize CO_2 emissions. The second and third objective functions, expressions (9) and (10), are related to the economic and social aspects of the proposed model. The presented mathematical model in this study considers both pick-up and delivery problems. Concerning the complexity of the proposed model, serving both pickup and delivery nodes is a straightforward task. Here, we intend to maximize the number of pick-up nodes that can be mentioned as the third objective function regarding the social aspect of the proposed model. Constraints (11) enforce the model to use lower than K vehicles; expressions (12–13) are the vehicle flow conservation constraints for all delivery nodes, and similarly, expressions (14–15) are the vehicle flow conservation constraints for some pickup nodes. Constraints (16) indicate that each vehicle serves only one type of nodes (delivery or pick-up). Constraints (17) are the commodity flow conservation constraints used in most VRP models, and constraints (18) and (19) ensure that the carried load of each vehicle to delivery and pick-up nodes does not exceed its capacity.

Constraints (20) confirm that the vehicle is traveling on the arc (i, j) to select one path and constraints (21) indicate that the vehicles traverse the arc (i, j) of the path $\wp_{ij}^{P}$ within exactly one time interval. Constraints (22) show that the total load carried on different paths of $\wp_{ij}^{P}$ is equal to the carried loads that must be transmitted from the node i to j. Constraints (23–24) guarantee that the carried load on one path does not exceed the capacity of the vehicle.

Constraints (25) indicate that the time of the vehicle departing from the depot is no earlier than the beginning of the time horizon ε, and likewise, expression (26) shows that the time of the vehicle returning to the depot does not exceed the end of the time horizon $\mathcal{L}$. Constraint (27) confines the lower and upper bounds of departure time within the time interval if $\wp_{ij}^{P}$ is selected; otherwise, $w_{ij}^{pm} = 0$. Constraints (28) compute the earliest possible departure time at the node j if the vehicle travels on the path $\wp_{ij}^{P}$. Constraints (29) indicate that all services must be completed within the delivery time horizon. Constraints (30) specify that all customer nodes must be served at their corresponding hard time windows. Ultimately, constraints (31–37) are used to define all variables. Note here that we retain constraints (18) for more clarification, and it would be redundant due to constraints (22–24).

To understand the complexity of the proposed mathematical model, a description of big (O) notation is presented. This kind of problem can be mentioned as a pickup and delivery problem (PDP). Because our proposed model uses the main assumptions of the PDP problem, it is a non-deterministic polynomial-time NP-hard problem. The complexity of the proposed mathematical model is as follows:

$$O\left(|\mathcal{N}^c|^2 . |K|\right), if \, |K| \geq \mathcal{N}^-,$$

$$O\left([|\mathcal{N}^c\mathcal{O}|]^2 . \mathcal{N}^-\right), if \, |K| \mathcal{N}^-,$$

As it has been proven to be an NP-hard problem, with an increase in the size of the problem, the complexity of solving this kind of problem increases exponentially. Therefore, in conjunction with the mentioned pitfall, specific preprocessing procedures must be handled to shrink the size of the network, which will be discussed in the following section.

6 Solution Methodology

This section presents the methodology used to solve the MOSVRP.

6.1 The network shrinking procedure (NSP) based on the Voronoi diagram

This study proposes a novel two-stage solution framework that integrates a geometric preprocessing heuristic with a primary optimization model. The motivation is to reduce computational complexity when dealing with large-scale spatial network design problems. The two main stages of the methodology are as follows: pre-processing via NSP and main optimization over a reduced network.

To reduce the solution space and accelerate the main optimization algorithm, we introduce a novel geometric heuristic called the NSP. This procedure filters and partitions the full network by exploiting spatial proximity among nodes using a Voronoi Diagram (VD), which decomposes the network area into proximity-based regions.

The VD is constructed over the set of demand or facility nodes $P = \{p_1, p_2, \ldots, p_n\}$ such that each node p_i defines a Voronoi cell $V(p_i)$, composed of all points in the plane closer to p_i than to any other node:

$$V(p_i) = \{q | dist(q, p_i) \leq dist(q, p_j), \forall p_j P\} \tag{38}$$

Here, $dist(q, p_i)$ represents the Euclidean distance between point q and node p_i. This geometric decomposition allows us to identify relevant local neighborhoods and prune unrelated nodes.

To further refine the neighbourhood structure, we define two key concepts:

- **Definition 1 (Voronoi Distance,**
- ***vd)***: The number of Voronoi cell boundaries (edges) crossed by a straight line connecting two points.
- **Definition 2 (k-ring Voronoi Neighbors)**
- : The set of nodes that are exactly k Voronoi distances away from a given node p_j, denoted as:

$$\begin{aligned} &vn(p_j, k) \\ &= \{y | vd(p_j, x) = k, y \in P, k \in \{1, 2, \ldots, \infty\}\}, P = \{p_1, \ldots, |P|\}. \end{aligned} \tag{39}$$

- Using these concepts, we limit the candidate solution space to only those nodes lying within a small k-ring neighborhood around each primary node. This enables the generation of a **reduced network**, which maintains spatial relevance while significantly lowering computational burden.

Figure 3 illustrates a Voronoi diagram and the corresponding k-ring regions for a selected node.

Once the reduced network is obtained through NSP, the main optimization model is solved using proposed metaheuristic approach This two-stage strategy ensures that: (*i*) The original problem size is shrunk before exact or heuristic search begins; (*ii*) Solution quality is preserved by keeping the most relevant candidate nodes based on geometric proximity; and (*iii*) Computational time is significantly reduced, enabling application to large-scale real-world networks.

This structured methodology effectively balances model complexity, solution accuracy, and computational tractability.

To construct localized neighborhoods around each customer node based on spatial proximity, we introduce Algorithm 1, which builds k-ring Voronoi sets for all nodes in the network. The goal is to identify all customers that lie within k Voronoi boundaries from a given customer node, thereby forming a geometrically meaningful reduced neighborhood structure.

To reduce computational complexity and localize the optimization process in large-scale spatial problems, we propose a k-ring Voronoi neighborhood construction algorithm. This algorithm identifies spatially close neighbours of each customer node based on Voronoi partitions and iteratively builds ring-based proximity sets. These localized neighbourhoods form the foundation of the NSP and enable a tractable solution approach.

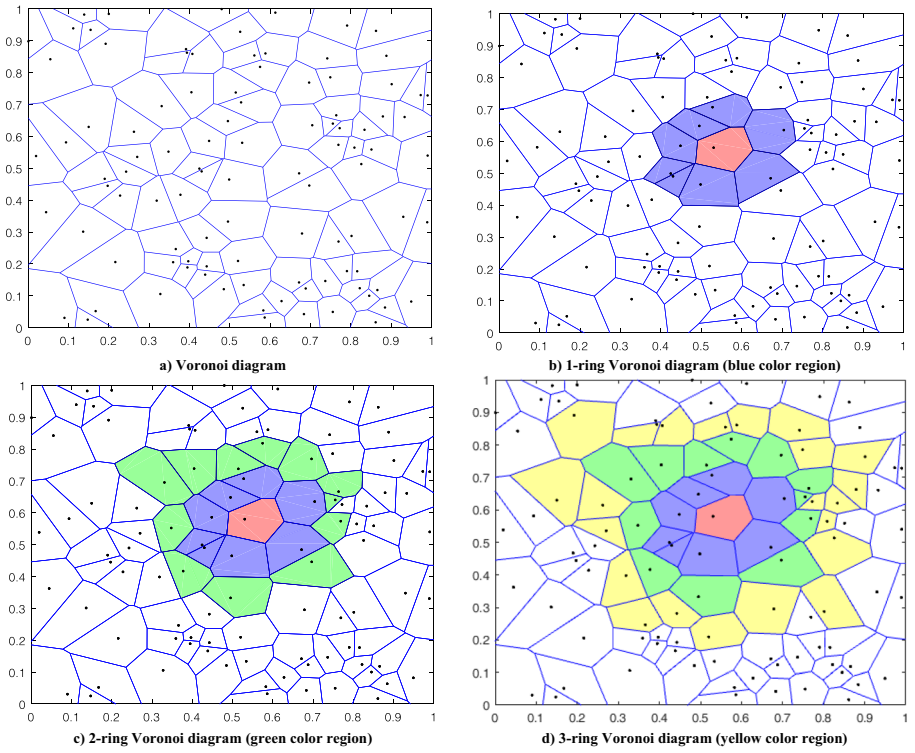

Fig. 3 K-ring Voronoi diagram

Given a set of customer nodes $C = \{C(1), C(2), \ldots, C(|C|)\}$ distributed across a two-dimensional plane, we first construct a Voronoi diagram, which divides the plane into non-overlapping convex cells. Each cell corresponds to a single customer node and includes all points in the plane that are closer to that node than to any other.

Let $Edge(C(i))$ denote the set of polygonal edges that define the Voronoi region (cell) surrounding the customer $C(i)$. These edges form the basis for identifying adjacency relationships among Voronoi cells.

The k-ring Voronoi neighbourhood for the customer $C(i)$, denoted R_{ik}, is defined as the set of customer nodes that lie at an exact Voronoi distance k from $C(i)$. The Voronoi distance is defined as the number of Voronoi cell edges that must be crossed to move from $C(i)$ to another customer node.

The goal of Algorithm 1 is to construct the full sequence of k-ring neighbourhoods $R_{i1}R_{i2}, \ldots$ for each customer node $C(i)$, until all customers have been included or a predefined neighbourhood depth k_{max} is reached.

This algorithm is central to the NSP because it identifies localized customer clusters that are spatially relevant to each node. By limiting the search space for routing, allocation, or service to only nearby neighbors within a defined k-ring, we achieve several goals. First, instead of solving optimization over the full set of customer nodes, we focus on a smaller, geometrically relevant subset. Second, the reduced neighbourhood structures require fewer variables and constraints, enhancing the speed of any subsequent exact or heuristic optimization model. And third, Voronoi-based grouping ensures that proximity and travel efficiency are respected in the reduced model.

Given that fuel consumption is directly related to travel distances and path selection, this k-ring construction also supports the evaluation of cost-effective neighborhoods. The reduced regions generated by the algorithm will later serve as input to fuel-efficient path selection, where longer-distance and low-priority customers can be excluded from certain decision stages. To reduce the size of the network while preserving spatial and topological relevance for optimization, we now present the NSP. This method integrates the Voronoi-based k-ring structure (from Algorithm 1) with shortest path computations to retain only the most relevant connections for each customer over a set of time slots.

The NSP iteratively explores a growing neighbourhood around each customer and preserves only those paths that are necessary for efficient routing. Redundant and unreachable paths are eliminated. The result is a significant reduction in the number of considered arcs and nodes, making the subsequent optimization problem tractable on larger networks.

NSP is designed to efficiently reduce the scale of the optimization problem by identifying a subset of spatially and temporally relevant shortest paths for each customer node. It operates over a predefined time horizon T and a set of customer nodes C, using the k-ring Voronoi neighborhoods R_{ik} generated from Algorithm 1. For each time slot $t \in T$ and each customer $i \in C$, the algorithm initializes a path matrix P_i^t, filled with infinity values to represent initially unknown distances. The procedure starts with the 1-ring Voronoi neighborhood R_{i1} , defining it as the initial set of boundary nodes BN whose paths from node iii will be computed first. For $k = 1$, the algorithm computes and stores the shortest path $\wp(i, j)$ from node iii to each node $j \in BN$ in the matrix P_i^t. For $k > 1$, the algorithm proceeds iteratively, initializing a binary vector BR to track blocked nodes and a set H to store neighbors that are part of redundant paths. For each node $j \in R_{ik}$, it calculates the shortest path $\wp(i, j)$, updates the corresponding value in P_i^t, and checks whether any already-discovered

node $s \in BN$ lies along the path. If so, the 1-ring neighborhood of $BN\ (s)$ is computed and added to H, while marking the corresponding node in BR. After all nodes in R_{ik} are processed, the set BN is updated to include $R_{ik} \cup H$, and the algorithm checks the termination condition: if all nodes in the current ring are marked as blocked in BR, the procedure ends for node iii and time slot t. Otherwise, k is incremented, and the process repeats with the next ring $R_{i(k+1)}$. The final output is a reduced path matrix P_i^t for each node and time slot, containing only the shortest paths to relevant neighbors. This structure provides a localized, time-sensitive, and computationally efficient representation of the network that supports scalable optimization without compromising on spatial precision or path diversity.

6.2 Extended multi-objective volleyball premier league algorithm

We use the Volleyball Premier League (VPL) algorithm, which was implemented based on the concepts of a volleyball tournament (Moghdani & Salimifard, 2018). Later, the multi-objective version of this algorithm, named multi-objective VPL (MOVPL) (Moghdani et al., 2020), was introduced based on the leader selection strategy. We propose the reference point approach, the disruption operator, and several VRP operators in the following.

6.2.1 Reference point approach

This part is devoted to elucidating the main structure based on the reference point (MOVPL-RP). To date, various methods have been developed and introduced to cope with multi-objective functions in MOEAs. We use the reference point concept used in NSGA-III. The execution of MOVPL follows the main structure of the basic VPL algorithm, which performs the reference point concept. We propose the MOVPL algorithm, as shown in Algorithm 3.

In what follows, we will describe the main concepts and modules which are used in the reference point approach.

Determination of reference points on a hyper-plane: The most significant drawback of standard MOEAs that used the classical approach in Pareto domination is the lower diversity obtained solution. To cope with this issue, an advanced approach is suggested to apply a predefined set of reference points that are highly distributed in the search space. This approach, named reference point, was first used by (Deb & Jain, 2014) in NSGA-III. Note that a set of reference points can be determined using a specific procedure or preferentially by experts. We use Das & Dennis's method (Das & Dennis, 1998) to determine the reference points in the hyperplane. Therefore, for any problem with M-objective and p division, the following formula is given to compute the total number of reference points:

$$H = \begin{pmatrix} M+p-1 \\ p \end{pmatrix} or H = \begin{pmatrix} M+p-1 \\ M-1 \end{pmatrix} \tag{40}$$

Adaptive normalization of population members: The main criterion for selecting individuals in all MOEAs is domination, which is obtained based on the Pareto front. Therefore, for any iteration, after implementing operators, all parents and offspring are combined, and finally, the best individuals within the population size are selected for the next generation. In this approach, once the solutions have the same rank in the Pareto frontier, we perform the reference point approach to choose better solutions, which guarantees higher diversity solutions.

In this approach, we first determine the optimal points with the following formula:

$$\overline{z} = \left(z_1^{min}, z_2^{min}, \ldots, z_M^{min}\right) \tag{41}$$

where z_M^{min} is the best value of obtained M th objective function. After obtaining the ideal point $\overline{z}$, we measure f_i with the following formula:

$$f_i\prime = f_i\left(x\right) - z_i^{min} \tag{42}$$

Subsequently, we determine the extreme point of all objectives to form an achievement scalarizing function (ASF). In this approach, ASF is computed as follows:

$$\begin{aligned} &ASF\left(x, w\right) = max_{i=1}^{m}\left(\frac{f_i\prime\left(x\right)}{w_i}\right) or \\ &max_{i=1}^{m}\left(\frac{f_i\left(x\right) - z_i^{min}}{w_i}\right) for x \in S_t \end{aligned} \tag{43}$$

where w_i illustrates the weight vectors for corresponding objective functions and the S_t is related to the new population at iteration t, and x^* is obtained with the following formula:

$$x^* = argmin ASF\left(x, w\right) \tag{44}$$

Then, the z_i^{max}, denoting the maximum value of i th objective, is computed as follows:

$$z_i^{max} = f_i\left(x^*\right) - z_i^{min} \tag{45}$$

In the reference point approach, we use extreme points for all objective functions (z_i^{min} and z_i^{max}) to normalize individuals. Therefore, we use the following formula, as the most common approach for scalarizing, to normalize the individuals:

$$f_i^{normal}\left(x\right) = \frac{f_i\left(x\right) - z_i^{min}}{z_i^{max} - z_i^{min}} for i = 1, 2, \ldots, m \tag{46}$$

The general framework of the normalizing procedure, as the initial step of the reference point approach, is illustrated in Algorithm 4.

Association operation: The second stage of the reference point approach is related to association operation, in which all individuals in the Pareto front are assigned to a reference point. To reach this goal, we connect each reference point with the origin to make a set of reference lines. Next, we measure the perpendicular distance of individuals in the population from each reference line to determine which reference line has the nearest distance to any individual. Thus, all the individuals are associated with one of the reference lines. The procedure of the association operation is depicted in Algorithm 5.

Niche-preservation operation: In this part, we describe the niche-preservation operation to decide which individuals will be retained for the next iteration. To create a criterion for selecting individuals, we define niche count as ρ_j for the j th reference point. At the first step of this operator, the reference point with the minimum value of ρ_j is selected. If there is

more than one reference point that has the minimum value of ρ_j, we select one of them randomly. In the case of $\rho_j = 0$, there have been two possible cases that must be considered. In the first case, once there is more than one member, the one that has the lower perpendicular distance from the reference line is selected for the next iteration, and eventually, the value of ρ_j is added by one. In the second case, no member is associated with a reference line, so the corresponding reference line is discarded from further consideration. In the case $\rho_{\overline{j}} \geq 1$, an individual is randomly chosen to add a member, if one exists, from the front F_l that is associated with the reference point $\overline{j}$ is added to the next generation, P_{t+1}. The count $\rho_{\overline{j}}$ is then incremented by one ($\rho_j = \rho_j + 1$). After niche counts are updated, the procedure is repeated for a total of K times to fill all vacant population slots of P_{t+1} (or until the population size reaches N_{pop}).

Disruption operator: to improve and enhance the search space in continuous optimization, we intend to add a specific operator, termed the Disruption Operator (DO), which demonstrates its superior performance in many scientific areas of literature (see, e.g., (Neggaz et al., 2020)). Significantly, DO is not directly related to the reference point approach, and we add this operator to receive higher diversity in the continuous optimization search space. This operator mimics phenomena of astrophysics that augment the capability of metaheuristics for higher exploration in continuous search space. To apply this operator, the following mathematical relation is given.

$$DO = \begin{cases} \mathcal{D}_{ij} \times \lambda\left(-2, 2\right) if \mathcal{D}_{i,best} \geq 1, \\ 1 + \mathcal{D}_{i,best} \times \lambda\left(\frac{-10^{-4}}{2}, \frac{10^{-4}}{2}\right) otherwise. \end{cases} \tag{47}$$

where $\mathcal{D}_{ij}$ denotes the Euclidean distance between the i th member of the population and its closest neighborhood j th member of the population. Note that $\lambda\left(x, y\right)$ is a function that randomly generates a number between x and y. Line 16 of Algorithm 3 displays the disruption operator strategy used in the proposed approach, and more details of this operator are presented in Algorithm 7.

6.2.2 Embedding VRP heuristics to improve the solution

In this part, we present a comprehensive approach to improving the solutions based on a set of heuristics related to VRP problems. Overall, our proposed approach in this section is based on destroy and repair operators, initially used in Large Neighborhood Search, and further extended to Adaptive Large Neighborhood Search (ALNS). Therefore, this approach comprises a set of removal and insertion heuristics.

We use an adaptive weight adjustment (AWA) procedure to form a framework that iteratively improves the solutions. For selecting operators, we use the probabilities of operators based on their successful implementation to enhance solutions. At the initial stage, all operators have the same probability that they are $\frac{1}{|R|}$ and $\frac{1}{|I|}$ for removal and insertion, respectively. Note that R and I are the set of removal and insertion in this regard. For the remaining approach, the probability of operators is updated based on the roulette-wheel mechanism. Once an operator is selected, three conditions will occur, and the probability values of all operators are updated based on the obtained new score. Note that the probability value of each operator is defined as a fraction number $\frac{x}{y}$ where $x < y$. Let $Xnew$,$Xcur$

and X^* be a new solution obtained from the corresponding operator, current solution, and best solution, respectively. The following formula is given to update the probability:

$$p_t^i = \begin{cases} \frac{x+2}{y} if\ Xnew < X^*, \\ \frac{x+1}{y} if\ Xnew < Xcur, \\ \frac{x}{y+1} if\ Xnew \geq Xcur. \end{cases} \tag{48}$$

where p_t^i is the probability of the current operator in which $i \in I$, and a similar formulation can be adopted for removal operators. Subsequently, by obtaining the probability value of each operator, the corresponding value of probability for other operators is updated based on the most straightforward option of normalization as follows:

$$p_t^i = \frac{p_t^i}{\sum_{i \in I} p_t^i} \tag{49}$$

The above formula can be reconstructed for removal operators. In this approach, we perform the twelve removal operators, which are comprehensively used in the literature, including Random removal (RR), Worst-distance removal (WDR), Worst-time removal (WTR), Route removal (RoR), Shaw removal (SR), Proximity-based removal (PR), Time-based removal (TR), Demand-based removal (DR), Historical knowledge node removal (HR), Neighborhood removal (NR), Zone removal (ZR), and Node neighborhood removal (NNR). We also implement five insertion operators in this study, which include Greedy insertion (GI), Regret insertion (RI), Greedy insertion with noise function (GIN), Regret insertion with noise function (RIN), and Zone Insertion (ZI). For both kinds of operators, interested readers may refer to (Demir et al., 2012) for more details. The current approach is based on simulated annealing as a local search framework. Algorithm 8 shows the general framework of the proposed AWA approach using a combination of simulated annealing and heuristic operators to enhance solutions.

By adding Algorithm 8 to the proposed approach, as shown in Algorithm 3, our proposed approach, named MOVPL-RP-OD-AWA, is given for further consideration, and more experiments and analyses will be adopted to show the capability of this approach. In summary, the general framework used, as explained above, is shown in Fig. 4.

7 Numerical Experiments

The experimental settings, results, and sensitivity analysis are provided in this section.

7.1 Experimental design

We follow the same procedure as implemented in (Ehmke et al., 2016b; Huang et al., 2017; Qian & Eglese, 2016; Raeesi & Zografos, 2019), and used for London, Chicago, and Beijing. Also, we extend the procedure used in (Solomon, 1987) to generate customer graphs in

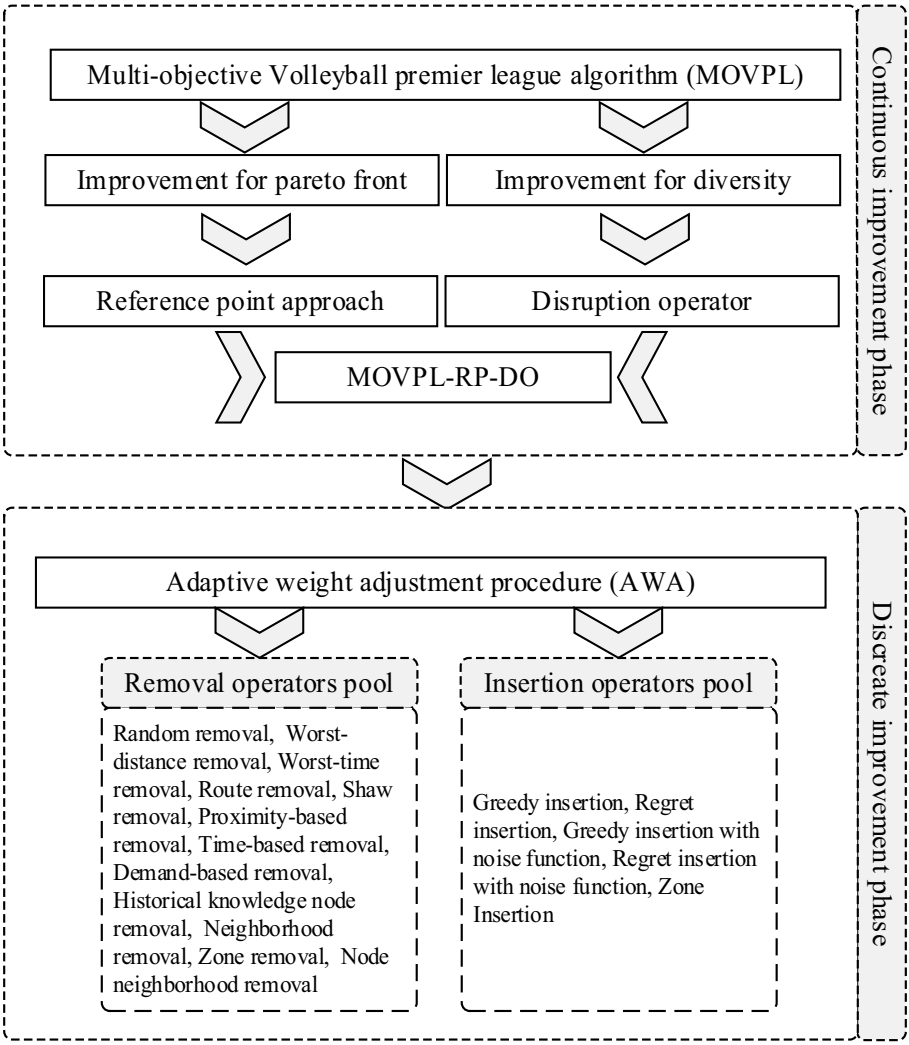

Fig. 4 The general framework for developing the methodology approach

Tehran. In the following subsection, the construction of the geographical graph used in this study is discussed in detail.

7.1.1 Network construction

The urban area of Tehran has been used as the geographical graph of this study. We consider roads in three groups, which is the typical approach in the literature (e.g., (Huang et al., 2017): residential roads, including local area, minor rural roads, minor intercity roads, and significant intercity roads; arterials, including minor arterials, major arterials, and expressways; arterial residential roads, arterials.

According to Fig. 5, most roads have vertical or horizontal directions, and we use Manhattan distance to measure traveling distances between nodes in an urban network. The urban area of Tehran contains 4986 arcs and 4323 nodes, representing the average speed of various types of roads in this study. Among all kinds of roads, the average speed and traffic conditions of the residential road are virtually steady throughout the day.

The customer graph of the current study is a set of 723 groceries and general merchandise retailers (red circles in Fig. 5) and a depot, highlighted in a black square.

Compared to cities such as Sydney or Amsterdam (as seen in www.tomtom.com), Tehran exhibits longer peak periods and lower average travel speeds, particularly in central corridors. However, the model's use of time-dependent speed profiles allows for easy adaptation. For example, Amsterdam's high share of bike traffic and regulated car access could be reflected by assigning consistently low congestion weights on key car routes and using modal share adjustments.

7.1.2 Test instances

We considered three kinds of instances, including R, C, and RC. For each category, we generated 30 instances. Let $TeCo$ be the general form of test instances, Te is equivalent to R, C, and RC, and Co is a set of index numbers equal to 01, 02, …, 30 for each kind of test instance. In the R instances, considered as the baseline instances, we randomly select N nodes among all customers. We also use the specific procedure to generate 30 instances for the C and RC categories presented in Appendix B For each test instance, the size of the problem is increased with the following formula:

$$|\mathcal{N}^c| = ACo + B, \tag{50}$$

where $|\mathcal{N}^c|$ denotes the number of customers in each test problem, A and B are constants equal to 3 and 6, respectively. We set the demand of each customer to 400 kg. In this study,

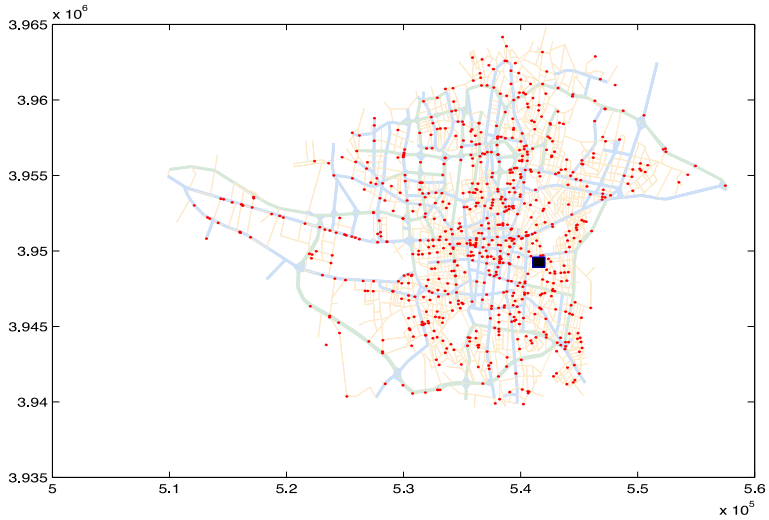

Fig. 5 The urban area of the city of Tehran

the homogeneous fleet is used to serve customers. Hence, following consultation from expert retailers, each fleet can serve ten customers in the best case; thus, we addressed the following relation to determine the number of homogeneous fleets for each test instance.

$$|K| = \frac{|\mathcal{N}^c|}{10} \tag{51}$$

The capacity of each fleet is set to 4460 kg, and we set the delivery time horizon from 6:00 to 18:00.

7.1.3 Experimental settings and computational environment

Hence, a new procedure is presented to reduce the urban network; we analyze the effect of the NSP algorithm on computational effort. We analyze the various kinds of MOEAs algorithms, including MOEA/D, MOPSO, MOVPL, MOVPL-RP, MOVPL-RP-DO, and MOVPL-RP-DO-AWA, to show the capability of the proposed approach. Table 3 above presents the parameter settings of the algorithms, which are obtained from (Moghdani et al., 2020).

We solved the instances using MATLAB software. All experiments were conducted on a server with Intel E5 4640, 2.4 GHz CPUs, and 64 × 8 GB memory. We also implemented a number of Pareto solution (NPS) and CPU time (CT) metrics as conducted in (Audet et al., 2018).

7.2 Computational results and analysis

The following subsections provide computational results and analysis of proposed approaches. The algorithms were implemented in MATLAB, version R2017a, and were run on a computer with 2.9 GHz AMD Ryzen 7 4800H processors and 32 GB of RAM. It is also noted that the presented mathematical model has been solved via IBM ILOG CPLEX, version 12.10.

7.2.1 The validation of the proposed mathematical model

In this subsection, we will provide an exact solution to the proposed mathematical problem in terms of all objective functions. Table 4 compares the extreme points obtained via the

Table 3 Parameter settings for the proposed algorithms

Algorithms	Parameters
MOVPL	$nPop = 100$, $T = 100$,$\lambda^f = 1.4$,$\lambda^s = 1.4$,$\psi^f = 1.4$,$\psi^s = 1.4$,$\beta = 4$,δ_{pr}=0.5,$\delta_{st} = 0.5$,δ_{tr}=0.5, $MaxIt = 400$,$nArchive = 50$
MOPSO	$\phi_1 = \phi_2 = 2.05$, $\phi = \phi_1 + \phi_2$, $w = \frac{2}{\phi - 2 + \sqrt{\phi^2 - 4\phi}}$ $c_1 = \omega \times \phi_1$, $c_2 = w \times \phi_2$, $\alpha = 0.1$, $\beta = 4$, $nGrid$=10
MOEA/D	$N = 100$, $T = 10$, $n_r = 1$, $\gamma = 0.9$, $m_r = 0.5$,$\eta = 30$

proposed approach, MOVPL-RP-DO-AWA, for five small test instances, from R01 to R05, and the results of a commercial solver.

All objectives have been reported in Table 4 to adopt the difference between the obtained extreme points and the exact feasible solutions. The relative error (RE) in all proposed objective functions is the burden between the heuristic approaches and the exact solutions of the MOSVRP, which have been used in this regard. The values of RE, as shown in the third column, demonstrate the percentage error in all objective functions obtained via the heuristics solution and the exact solution, which is computed as follows:

$$RE = \frac{z_i^a - z_i^*}{z_i^*} \times 100, i \in \{1, 2, 3\} \tag{52}$$

Where z_i^a and z_i^* denote the obtained extreme points via the proposed approach and an exact solution for the i th objective function, respectively. What stands out is that the proposed approach shows its exquisite performance in the third objective function. According to these figures in Table 4, the highest difference can be observed in the third test instance, R03, around 8 and 5.6% for the first and second objective functions, respectively. Concerning other elements pointed out in this table, it can be concluded that the measured REs have ranged from 2 to 5%.

7.2.2 Performance of the NSP

To show the performance of the proposed NSP, five test instances of each test cluster are selected and solved to optimality for the CO_2 emission minimization objective using the NSP-based MILP. We compare the solution used with the results obtained from non-NSP-based MILP, which computes the shortest path for the full set of required customer nodes. Table 5 shows the results obtained from this comparison. We provide several arcs (NA), minimization of CO_2 emissions, and CPU time to show how the NSP approach works effectively. A group of columns is devoted to showing the percentage difference between the two approaches.

In this table, we can observe that the proposed approach reduced the network size by 18.48% on average, and the improvement from using the proposed average has been obtained consistently by increasing the number of customers. Regarding environmental consideration, *Obj1* revealed that approximately 16.11% of test instances show that using NSP leads to promising results. The difference in implementing the NSP approach on CPU time is quite significant, and the running time is reduced by at least 22.98% using the above-mentioned approach.

Table 4 A comparison between the proposed approach and the exact solution

Test Instances	MOVPL-RP-DO-AWA			An exact solution			RE (%)		
	z_1	z_2	z_3	z_1	z_2	z_3	z_1	z_2	z_3
R01	19.95	156.25	3	18.85	149.84	3	5.84%	4.28%	0.00%
R02	22.94	171.17	3	21.26	163.88	3	7.90%	4.45%	0.00%
R03	21.85	188.08	4	20.23	178.12	4	8.01%	5.59%	0.00%
R04	30.55	234.58	4	29.79	229.61	4	2.55%	2.16%	0.00%
R05	29.59	246.58	6	28.26	233.51	6	4.71%	5.60%	0.00%

Table 5 The performance evaluation of using NSP

Test instances	with NSP			without NSP			Difference (%)		
	NA	Obj1(Lit)	CT(min)	NA	Obj1(Lit)	CT(min)	NA	Obj1(Lit)	CT(min)
R01	4240	19.95	11.66	4986	22.72	15.47	14.96	12.19	24.63
R02	3690	23.09	13.38	4986	24.31	16.79	25.99	5.02	20.31
R03	4270	24.06	15.62	4986	25.33	20.49	14.36	5.01	23.77
R04	3778	31.73	16.38	4986	40.16	21.18	24.23	20.99	22.66
R05	4089	19.99	10.28	4986	24.58	13.14	17.99	18.67	21.77
C01	3789	28.14	11.18	4986	39.60	14.41	24.01	28.94	22.41
C02	4111	24.05	13.67	4986	25.58	18.01	17.55	5.98	24.10
C03	4425	20.15	16.46	4986	25.42	19.87	11.25	20.73	17.16
C04	4512	29.28	17.65	4986	38.52	23.21	9.51	23.99	23.96
C05	3740	30.63	11.83	4986	37.35	16.87	24.99	17.99	29.88
RC01	4388	18.62	14.91	4986	21.91	18.27	11.99	15.02	18.39
RC02	4325	21.01	15.57	4986	26.59	19.12	13.26	20.99	18.57
RC03	3690	23.85	13.86	4986	27.41	19.65	25.99	12.99	29.47
RC04	3811	30.56	18.74	4986	34.34	21.33	23.57	11.01	12.14
RC05	4111	31.01	18.11	4986	39.88	28.12	17.55	22.24	35.60

Table 6 Aggregated Wilcoxon Signed-Rank test of the NPS metric for all sets

Class	Result	MOVPL-RP-DO-AWA vs #					%
		MOEA/D	MOPSO	MOVPL	MOVPL-RP	MOVPL-RP-DO	
R	w	28	28	27	26	23	88.00
		1	2	3	4	5	10.00
		1	0	0	0	2	2.00
C	w	25	24	23	24	23	79.33
		2	3	4	2	2	8.67
		3	3	3	4	5	12.00
RC	w	27	28	25	26	24	86.67
		3	2	3	2	4	9.33
		0	0	2	2	2	4.00
Total		80/6/4	80/7/3	75/10/5	76/8/6	70/11/9	381/42/27

7.2.3 Performance of the proposed approaches

To show the efficacy of the proposed approach, Table 6, presented in Appendix C, provides different statistical descriptions of the statistical results of the NPS metric for class R. In the following, we consider the analysis comparison of the NPS metric for class R. The same procedure will be conducted for the other metrics (SP, MS, and CT) and classes of problem (C and RC).

We use the Wilcoxon Signed-Rank Test (Yu & Li, 2015) to show how the algorithm performs statistically. Therefore, the following relation is given for the null hypothesis (H_0) and alternative hypothesis (H_1):

$$\left\{ \begin{array}{l} H_0 : \mu_1 = \mu_2 \\ H_1 : \mu_1 \neq \mu_2 \end{array} \right\} \tag{53}$$

Table 7, which is placed in Appendix C shows the Wilcoxon Signed-Rank Test of the NPS metric for class R. This table provides four columns for comparison, where the first column, R+, indicates the sum of the ranks once the proposed algorithm outperforms its opponents. The second column, R-, denotes the sum of the ranks once the proposed algorithm is defeated by its rivals. The third column, p, represents the p-value for the statistical test. Finally, the fourth column, *h*, signifies the statistical results. According to this column, the appearance of "+1" means that the proposed algorithm outperforms its opponent statistically, and conversely, "-1" represents the opposite, where the performance of the other algorithm is better than our proposed approach. If there is no significant difference between the two algorithms, "0" is observed. Finally, the last row, indicated with $w/t/l$, is used to show the number of wins, ties, and losses, respectively, in the considered class of problems. As shown in Table 7, MOVPL-RP-DO-AWA has significantly outperformed at least 23 of 30 test instances (76%). Thus, there are three different kinds of problems, and Table 8 illustrates comprehensive results that indicate the overall performance of the proposed approach in this class of problems. According to this table, the proposed approach regarding NPS dominates at least 80% of problems in different classes. For the general view, MOVPL-RP-DO-AWA has outperformed 381 of 450 problems (79.37%), indicating the best performance of the current approach compared with others regarding the NPS metric.

Here, we provide Fig. 6 to illustrate the overall performance of the proposed approach in all metrics. As clearly shown, MOVPL-RP-DO-AWA. Figure 6 reveals the percentage of success by the proposed algorithm for all metrics, as we can see that the proposed approach defeats its rival by at least 72%. This figure shows an exception for CT metrics in that MOVPL-RP-DO-AWA cannot exceed the others above 50%. Bearing this in mind, the fact has arisen from implementing the various types of VRP heuristics, including removal and insertion operations. Implementing these operations in our approach leads to a running time being somewhat high; nevertheless, advantages in other metrics justify the implementation of AWA.

7.2.4 The Pareto front of the proposed model

We devote this subsection to analyzing the optimal Pareto front obtained from all approaches. As mentioned in Sect. 4, we propose an integrated approach based on the reference point

Table 7 Sensitivity analysis for R instances

Instance	Parameter varied	Values tested	Δz_1	Δz_2	Δz_3
R01	ψ_e	0.5×, 1×, 1.5×	+6.8%, 0%, −6.1%	+0.3%, 0%, −0.2%	0%, 0%, 0%
R07	Traffic speed	−20%, 0%, +20%	+10.5%, 0%, −8.2%	+6.3%, 0%, −4.9%	−4.0%, 0%, +3.3%
R13	Q	−20%, 0%, +20%	−2.5%, 0%, +1.8%	−1.0%, 0%, +0.6%	−9.1%, 0%, +9.9%
R20	ψ_e	0.5×, 1×, 1.5×	+7.1%, 0%, −5.6%	+0.2%, 0%, −0.3%	0%, 0%, 0%
R26	Traffic speed	−20%, 0%, +20%	+9.8%, 0%, −6.7%	+5.5%, 0%, −3.9%	−3.7%, 0%, +3.4%

Table 8 Sensitivity analysis for C instances

Instance	Parameter varied	Values tested	Δz_1	Δz_2	Δz_3
C03	ψ_e	0.5×, 1×, 1.5×	+4.9%, 0%, −4.4%	+0.1%, 0%, −0.1%	0%, 0%, 0%
C08	Traffic speed	−20%, 0%, +20%	+7.6%, 0%, −6.5%	+3.9%, 0%, −3.1%	−2.7%, 0%, +2.1%
C14	Q	−20%, 0%, +20%	−1.8%, 0%, +1.6%	−0.7%, 0%, +0.5%	−6.8%, 0%, +7.6%
C22	ψ_e	0.5×, 1×, 1.5×	+5.3%, 0%, −4.2%	+0.1%, 0%, −0.1%	0%, 0%, 0%
C30	Traffic speed	−20%, 0%, +20%	+8.2%, 0%, −6.8%	+4.4%, 0%, −3.5%	−3.2%, 0%, +2.5%

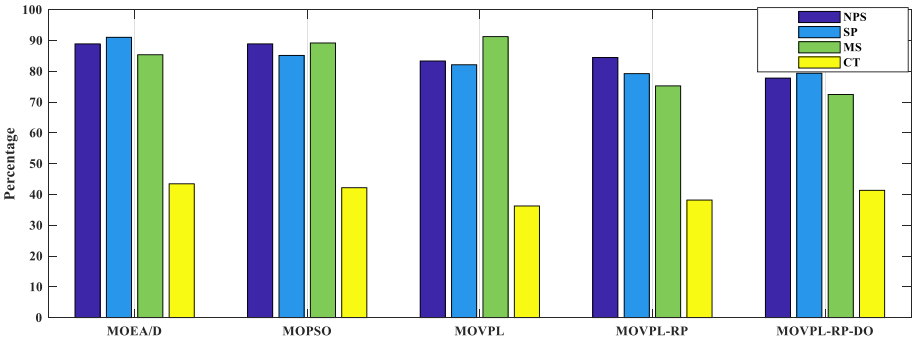

Fig. 6 The overall performance of the proposed approach to beat its rivals in terms of several metrics

concept, disruption strategy, and AWA to generate optimal Pareto fronts. Table 9, as seen in Appendix C shows the extreme point of each objective function of the test instance R, and detailed results of other types of instances are provided in an additional file. In these tables, three columns, named z_1, z_2, and z_3, are given for the global optimum of the first objective (fuel consumption in liters), second objective (distance in km), and third objective (number of served to pick-up nodes), respectively.

Table 9 shows extreme points on the Pareto fronts for all the proposed approaches in a class R test instance. It is clearly observed from this table that MOVPL-RP-DO-AWA shows a better performance in obtaining all considered objective functions. In the case of the fuel consumption found by the proposed approach, this is much less than is found by the others; the amount of fuel consumption has improved to 18.71% on average. In other cases, on average, the traveling distance and number served to pick-up nodes found by MOVPL-RP-DO-AWA are 11.92–18.25%, respectively, of those found by other proposed approaches.

Table 10 shows extreme points on the Pareto fronts for all proposed approaches in the class RC test instance. Comparable with the obtained results from Table 9, the proposed approach improves 96.44% of all objective functions on average. For example, the number of served pick-up nodes has increased by at least 17.76%, indicating the proposed approach's superior performance compared to its rivals.

Table 9 Sensitivity analysis for RC instances

Instance	Parameter varied	Values tested	Δz_1	Δz_2	Δz_3
RC05	ψ_e	0.5×, 1×, 1.5×	+6.2%, 0%, −5.5%	+0.3%, 0%, −0.2%	0%, 0%, 0%
RC09	Traffic speed	−20%, 0%, +20%	+9.3%, 0%, −7.6%	+5.1%, 0%, −4.2%	−3.9%, 0%, +3.6%
RC16	Q	−20%, 0%, +20%	−2.4%, 0%, +2.1%	−0.9%, 0%, +0.7%	−7.7%, 0%, +8.3%
RC23	ψ_e	0.5×, 1×, 1.5×	+6.5%, 0%, −5.2%	+0.2%, 0%, −0.2%	0%, 0%, 0%
RC28	Traffic speed	−20%, 0%, +20%	+9.1%, 0%, −7.2%	+4.8%, 0%, −4.0%	−3.6%, 0%, +3.3%

Table 11 indicates extreme points on the Pareto fronts for all proposed approaches in a class C test instance. As anticipated, this table reveals that extreme points of the proposed approach, the individuals with minimum fuel consumption, distance, and maximum served to pick-up nodes, could be found through the proposed approach. Regarding this table, MOVPL-RP-DO-AWA has improved the obtained solution by at least 17.93% on average for all extreme points of Pareto fronts.

We now present the general comparison between the proposed algorithm and its rivals in obtaining extremely dominant solutions for all objective functions. Note that the general form of the *x*-axis is $z\alpha\beta$, where α denotes the index of objective functions, equals to $\{1, 2, 3\}$, β signifies the index of rivals of the proposed approach, and $\beta = \{1, 2, .., 5\}$, which are equal to MOEA/D, MOPSO, MOVPL, MOVPL-RP, and MOVPL-RP-DO, respectively.

Results obtained from Fig. 7 demonstrate that in seven objectives out of 15 (three objectives for five algorithms), the proposed approach can resolve all test problems in all classes, which proves the capability of MOVPL-RP-DO-AWA to reach extreme points of Pareto solutions. We can also see the superiority of the proposed approach in seven objective functions, in which extreme points of 25 out of 30 (83%) test instances belong to MOVPL-RP-DO-AWA.

7.2.5 Sensitivity analysis

To examine the robustness of the proposed mathematical model, we conducted a sensitivity analysis on key input parameters that have the potential to significantly influence solution quality and objective trade-offs, including ψ_e, traffic speed profiles, and the capacity of a vehicle (Q). The baseline instance is defined using average traffic speed data extracted from Tehran's road network, along with nominal values for environmental weights based on standard carbon emission conversion factors. We varied one parameter at a time while keeping others constant and recorded the percentage change in each of the three objectives, which are shown in the following tables.

As shown in Table 12, the R instances demonstrate the highest variation in emissions and travel distances when traffic speed changes, indicating their sensitivity to congestion due to scattered spatial distribution. Changes in the environmental weight (ψ_e) affect only

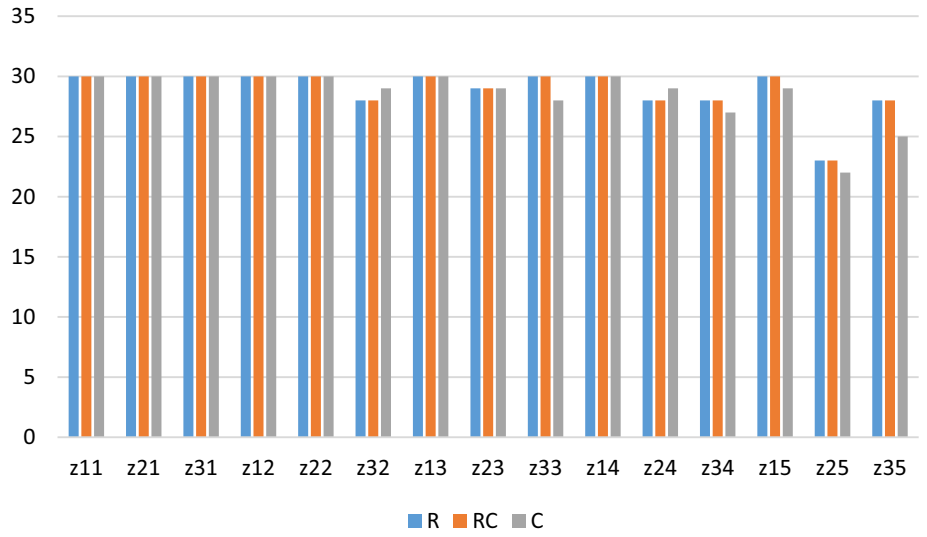

Fig. 7 The number of problems that the proposed algorithm outweighs its rival

emissions, as expected. Varying the capacity limit has a strong impact on z_3 confirming the model's ability to balance operational feasibility and social objectives.

As seen in Table 13, C instances show more stable behavior under speed variations due to shorter travel distances and denser routing. Emission weights (ψ_e) again impact only z_1, confirming the model's separability. Capacity constraints influence the social objective (z_3) significantly, though with slightly less magnitude than in R instances due to denser spatial structure allowing easier feasibility.

In Table 14, the RC instances show hybrid sensitivity characteristics. Their moderate responses to traffic speed and environmental weights place them between the R and C instances. This supports the model's capacity to adapt across diverse spatial layouts, maintaining predictable and interpretable behavior (Table 15)

8 Conclusion

This study has introduced a novel and comprehensive framework for addressing the Multi-Objective Sustainable Vehicle Routing Problem (MOSVRP) in congested urban environments. The model reflects the complex trade-offs inherent in real-world urban logistics by integrating economic, environmental, and social sustainability objectives, namely cost minimization, GHG emissions reduction, and customer satisfaction.

To manage the computational challenges of large-scale networks, we introduced a Voronoi diagram-based NSP, which significantly reduced problem size while preserving solution quality. Additionally, we enhanced the MOVPL algorithm with reference point guidance, disruption operators, and adaptive weight adjustment. This hybrid metaheuristic demonstrated superior performance in generating diverse, high-quality Pareto-optimal solutions. The proposed approach outperformed benchmark algorithms and exact methods across all key metrics when applied to Tehran's urban freight network. It achieved notable

reductions in fuel consumption and travel distance, while also increasing service coverage to pickup nodes.

The results of the sensitivity analysis across R, C, and RC instance categories demonstrate the robustness and adaptability of the proposed MOSVRP model. Changes in the environmental weight coefficient had a significant effect on GHG emissions while leaving travel distance and social benefit virtually unchanged, indicating that environmental priorities can be adjusted without disrupting operational performance. Variations in traffic speed affected all objectives, particularly in R and RC instances, where more dispersed customer locations made routing more sensitive to congestion, while C instances showed greater stability due to compact clustering. Adjusting the maximum capacity directly influenced the social objective, with minimal impact on emissions or travel distance, suggesting that social responsibility can be improved at a low operational cost. Overall, the model shows consistent and interpretable responses to key parameters, reinforcing its applicability across diverse spatial configurations and urban policy settings.

The results highlight the practical value of combining spatial heuristics with advanced metaheuristics for sustainable urban logistics. The framework is scalable, adaptable, and transferable to other metropolitan areas facing similar challenges. It offers a robust decision-support tool for logistics planners and policymakers aiming to balance operational efficiency with environmental and social responsibility. Therefore, our modeling framework is not limited to Tehran; it can be adapted to any urban setting through localized traffic speed data, making it applicable for a wide range of cities with different traffic regimes and planning needs.

Future research could investigate hybrid matheuristic approaches to further enhance solution reliability, incorporate real-time traffic data, and adapt the model to dynamic and stochastic environments. Integrating real-world datasets and stakeholder preferences would also improve the system's practical relevance for smart city logistics planning.

Appendix

Appendix A: Details of the CMEM model

We now present more details of the CMEM model. According to Eq. (1), the CMEM model has three coefficients that can be calculated as follows

$$\psi_e = \lambda k N_e V \tag{54}$$

$$\psi_s = \lambda \gamma \beta \tag{55}$$

$$\psi_w = \lambda \gamma \alpha \tag{56}$$

$$\psi_e = \lambda k N_e V$$

$$\psi_s = \lambda \gamma \beta$$

$$\psi_w = \lambda \gamma \alpha$$

where $\lambda = \frac{\varepsilon}{(\kappa\psi)}$, $\gamma = \frac{1}{(1000\varpi)}$,$\alpha = g\sin(\phi) + gC_r\cos(\phi)$ and $\beta = 0.5C_dA_f\rho$. Finally, we describe the parameters and the corresponding values based on a typical light-duty vehicle.

Appendix B: Generating test instances

We generate three kinds of test instances, termed R (random), C (clustered), and RC (random clustered). The number of customers, a significant part of generating test instances, is computed by Eq. (50). For R instance, we randomly select $|\mathcal{N}^c|$ nodes among all customer nodes. For C instance, we provide Algorithm B.1, with a maximum distance $\mathcal{D}$ that is 0.1 of the maximum possible distance between two nodes in the plane. So, we have:

$$\mathcal{D} = 0.1\sqrt{(\max(y) - \min(y))^2 + (\max(x) - \min(x))^2} \tag{57}$$

A lower bound and upper bound of the number of clusters are also determined with $\underline{\mathcal{C}} = 2$ and $\overline{\mathcal{C}} = 4$.

To construct RC instances, after determining the number of customers, half of the nodes are selected based on Algorithm B.1, and the others are selected randomly. Figures B.1 to B.3 show the generated C, R, and RC instances, respectively. Note that 25% of selected nodes are considered pick-up nodes, and the remaining are delivery nodes. The distribution of all types of instances is provided in an additional file.

Appendix C: Detailed results of R instance

Table 10 Description of CMEM model

Description	Notation	values
Fuel-to-air mass ratio 1	ε	1
Engine friction factor (kilojoule/rev/liter)	k	0.2
Engine speed (rev/second)	N_e	33
Engine displacement (liters)	V	5
Gravitational constant (meter/second2)	g	9.81
Coefficient of aerodynamic drag	C_d	0.7
Air density (kilogram/meter3)	ρ	1.2041
Frontal surface area (meter2)	A_f	3.912
Road angle	ϕ	0
Coefficient of rolling resistance	C_r	0.01
Vehicle drive train efficiency	ε	0.4
Efficiency parameter for diesel engines	ϖ	0.9
The heating value of typical diesel fuel (kilojoule/gram)	κ	44
Conversion factor (gram/second to liter/second)	ψ	737

Table 11 The statistical results of the NPS metric for set R

Test instances	MOEA/D				MOPSO				MOVPL				MOVPL-RP				MOVPL-RP-DO				MOVPL-RP-DO-AWA			
	Mean	Std	Best	Worst	Mean	Std	Best	Worst	Mean	Std	Best	Worst	Mean	Std	Best	Worst	Mean	Std	Best	Worst	Mean	Std	Best	Worst
R01	55.72	5.28	61	50	62.34	5.66	68	57	71.48	4.52	76	66.96	96.18	3.48	100	93	96.18	5.36	100	89	95.5	4.33	100	91
R02	61.64	4.36	66	57	65.87	3.13	69	63	65.37	6.63	72	58.74	95.12	3.98	99	91	95.12	6.88	98	86	94.09	5.91	100	88
R03	67.39	3.61	71	64	67.85	3.15	71	65	73.67	4.33	78	69.34	92.51	3.63	100	93	92.51	5.42	100	89	94.41	5.59	100	89
R04	58.55	6.45	65	52	60.1	5.9	66	54	76.72	6.28	83	70.44	95.17	4.75	98	89	95.17	3.19	100	94	95.83	4.17	100	92
R05	56.72	5.28	62	51	68.52	4.48	73	64	68.35	4.65	73	63.7	91.18	6.82	100	86	91.18	5.2	100	90	94.47	5.53	100	89
R06	57.84	4.16	62	54	67.66	4.34	72	63	68.2	5.8	74	62.4	94.15	4.13	100	92	94.15	3.88	100	92	94.84	5.16	100	90
R07	67.38	4.62	72	63	66.19	3.81	70	62	78.87	4.13	83	74.74	97.13	6.42	100	87	97.13	6.19	99	88	93.36	6.64	100	87
R08	62.12	6.88	69	55	58.09	6.91	65	51	64.33	5.67	70	58.66	99.18	3.4	100	93	99.18	5.56	100	89	93.33	6.67	100	87
R09	63.44	4.56	68	59	63.67	3.33	67	60	71.66	3.34	75	68.32	93.12	5.99	98	86	93.12	6.8	100	86	93.11	6.89	100	86
R10	63.22	5.78	69	57	62.33	6.67	69	56	66.6	5.4	72	61.2	91.19	6.85	100	86	91.19	5.79	100	88	96.28	3.72	100	93
R11	60.46	3.54	64	57	69.9	3.1	73	67	69.69	6.31	76	63.38	95.58	6.67	100	87	95.51	3.87	100	92	93.19	6.81	100	86
R12	63.74	4.26	68	59	62.51	3.49	66	59	65.56	4.44	70	61.12	93.14	5.41	94	83	9315	4.46	100	91	95.04	4.96	100	90
R13	64.73	5.27	70	59	60.62	4.38	65	56	73.2	4.8	78	68.4	96.45	5.94	100	88	96.18	3.12	100	94	94.74	5.26	100	89
R14	57.04	6.96	64	50	67.42	5.58	73	62	67.48	6.52	74	60.96	94.47	6.81	100	86	94.96	3.7	100	93	93.09	6.91	100	86
R15	55.02	6.98	62	48	58.34	6.66	65	52	77.15	4.85	82	72.3	93.58	3.39	98	91	93.53	3.96	100	92	95.77	4.23	100	92
R16	58.02	5.98	64	52	61.36	6.64	68	55	74.22	6.78	81	67.44	96.57	3.99	100	92	96.54	4.1	99	92	95.39	4.61	100	91
R17	57.31	5.69	63	52	68.7	4.3	73	64	72.08	4.92	77	67.16	93.14	6.32	97	84	93.43	5.69	100	89	93.19	6.81	100	86
R18	60.19	6.81	67	53	63.27	4.73	68	59	64.82	5.18	70	59.64	94.18	3.37	100	93	94.32	3.11	100	94	93.16	6.84	100	86
R19	64.83	5.17	70	60	63.53	6.47	70	57	80.65	3.35	84	77.3	96.58	3.3	100	93	96.52	6.91	100	86	95.66	4.34	100	91
R20	63.67	6.33	70	57	69.45	5.55	75	64	67.6	6.4	74	61.2	97.59	6.68	100	87	97.51	3.36	100	93	95.53	4.47	100	91
R21	69.01	3.99	73	65	64.44	4.56	69	60	68.23	4.77	73	63.46	93.96	6.8	95	81	93.36	5.74	100	89	93.06	6.94	100	86
R22	57.11	5.89	63	51	62.72	5.28	68	57	75.72	6.28	82	69.44	96.87	3.42	100	93	96.12	6.2	100	88	93.68	6.32	100	87
R23	68.33	5.67	74	63	64.62	6.38	71	58	64.02	6.98	71	57.04	93.58	6.37	100	87	93.14	3.83	100	92	96.34	3.66	100	93
R24	60.55	4.45	65	56	63.31	5.69	69	58	75.22	4.78	80	70.44	93.59	5.5	93	82	93.51	5.87	100	88	96.12	3.88	100	92
R25	64.61	4.39	69	60	70.75	4.25	75	67	71.28	3.72	75	67.56	95.58	4.68	100	91	95.55	5.43	100	89	96.57	3.43	100	93
R26	70.46	4.54	75	66	61.89	4.11	66	58	69.48	4.52	74	64.96	95.98	5.78	100	88	95.14	4.23	100	92	95.16	4.84	100	90
R27	65.26	4.74	70	61	65.51	4.49	70	61	78.88	3.12	82	75.76	95.78	4.22	96	88	95.78	4.45	100	91	93.63	6.37	100	87

Table 11 (continued)

Test instances	MOEA/D				MOPSO				MOVPL				MOVPL-RP				MOVPL-RP-DO				MOVPL-RP-DO-AWA			
	Mean	Std	Best	Worst	Mean	Std	Best	Worst	Mean	Std	Best	Worst	Mean	Std	Best	Worst	Mean	Std	Best	Worst	Mean	Std	Best	Worst
R28	62.04	4.96	67	57	66.55	5.45	72	61	74.38	6.62	81	67.76	96.58	6.85	100	86	96.59	6.49	100	87	96.12	3.88	100	92
R29	65.24	4.76	70	60	65.68	6.32	72	59	71.77	6.23	78	65.54	93.99	5.71	100	89	93.54	6.9	100	86	94.79	5.21	100	90
R30	63.73	3.27	67	60	65.83	3.17	69	63	70.4	4.6	75	65.8	93.58	4.43	100	91	92.58	6.57	100	87	94.11	5.89	100	88

Table 12 Wilcoxon signed-rank test of the NPS metric for set R

Test instances	MOVPL-RP-DO-AWA vs #																			
	MOEA/D				MOPSO				MOVPL				MOVPL-RP				MOVPL-RP-DO			
	R+	R-	*p*	*h*	R+	R-	*p*	*h*	R+	R-	*p*	*h*	R+	R-	*p*	*h*	R+	R-	*p*	*h*
R01	1149	681	0.03	+1	1138	692	0	+1	1183	647	0	+1	1126	704	0.04	+1	1085	745	0.05	+1
R02	1123	707	0.04	+1	1263	567	0.03	+1	1091	739	0.02	+1	1085	745	0.04	+1	695	1135	0.05	-1
R03	923	907	0.15	0	980	850	0.01	+1	1214	616	0.01	+1	1247	583	0.05	+1	1208	622	0.03	+1
R04	1140	690	0.01	+1	1222	608	0.01	+1	1048	782	0.01	+1	1087	743	0.03	+1	1018	812	0.04	+1
R05	1020	810	0.01	+1	1254	576	0.00	+1	1152	678	0.03	+1	1044	786	0.04	+1	1259	571	0.04	+1
R06	1008	822	0.01	+1	1064	766	0.00	+1	1199	631	0.03	+1	1291	539	0.02	+1	1126	704	0.01	+1
R07	1257	573	0.02	+1	1024	806	0.05	+1	969	861	0.05	+1	1341	489	0.01	+1	1066	764	0.01	+1
R08	957	873	0.05	+1	1271	559	0.03	+1	1327	503	0.03	+1	1091	739	0.01	+1	830	1000	0.02	-1
R09	1176	654	0.03	+1	1190	640	0.02	+1	1259	571	0.02	+1	953	877	0.01	+1	1159	671	0.05	+1
R10	1028	802	0.01	+1	1304	526	0.01	+1	1349	481	0.12	0	1188	642	0.04	+1	1052	778	0.05	+1
R11	1180	650	0.04	+1	1260	570	0.02	+1	1306	524	0.08	0	1131	699	0.01	+1	1018	812	0.01	+1
R12	1108	722	0.01	+1	1254	576	0.05	+1	1026	804	0.05	+1	1100	730	0.05	+1	1044	786	0.01	+1
R13	725	1105	0.02	-1	1350	480	0.01	+1	1347	483	0.03	+1	1078	752	0.03	+1	1342	488	0.00	+1
R14	1186	644	0.05	+1	1299	531	0.00	+1	982	848	0.00	+1	1145	685	0.04	+1	1215	615	0.05	+1
R15	1070	760	0.01	+1	1285	545	0.03	+1	1163	667	0.11	0	1101	729	0.04	+1	1262	568	0.04	+1
R16	1218	612	0.01	+1	1132	698	0.01	+1	1321	509	0.01	+1	1347	483	0.00	+1	982	848	0.01	+1
R17	1109	721	0.01	+1	1324	506	0.02	+1	1257	573	0.02	+1	1164	666	0.00	+1	1254	576	0.05	+1
R18	1238	592	0.03	+1	1342	488	0.04	+1	1159	671	0.01	+1	1261	569	0.04	+1	1260	570	0.01	+1
R19	960	870	0.01	+1	1266	564	0.03	+1	1283	547	0.03	+1	1306	524	0.05	+1	1236	594	0.02	+1
R20	1088	742	0.03	+1	957	873	0.11	0	1143	687	0.03	+1	1028	802	0.01	+1	1198	632	0.05	+1
R21	1147	683	0.03	+1	951	879	0.09	0	1172	658	0.04	+1	993	837	0.03	+1	1313	517	0.02	+1
R22	1066	764	0.00	+1	914	916	0.15	0	1056	774	0.04	+1	1062	768	0.03	+1	1262	568	0.12	0
R23	1224	606	0.01	+1	1073	757	0.01	+1	981	849	0.01	+1	1155	675	0.03	+1	1074	756	0.02	+1
R24	1062	768	0.02	+1	1335	495	0.01	+1	1236	594	0.03	+1	1206	624	0.04	+1	1064	766	0.13	0
R25	1199	631	0.01	+1	1250	580	0.01	+1	1019	811	0.01	+1	1290	540	0.01	+1	1261	569	0.05	+1
R26	1035	795	0.01	+1	1165	665	0.02	+1	1252	578	0.01	+1	1120	710	0.13	0	1296	534	0.13	0

Table 12 (continued)

Test instances	MOVPL-RP-DO-AWA vs #																			
	MOEA/D				MOPSO				MOVPL				MOVPL-RP				MOVPL-RP-DO			
	R+	R-	p	h	R+	R-	p	h	R+	R-	p	h	R+	R-	p	h	R+	R-	p	h
R27	1163	667	0.03	+1	1039	791	0.02	+1	1343	487	0.02	+1	1022	808	0.1	0	1188	642	0.15	0
R28	953	877	0.04	+1	1014	816	0.02	+1	981	849	0.02	+1	1004	826	0.06	0	1276	554	0.13	0
R29	1066	764	0.01	+1	1023	807	0.03	+1	1081	749	0.05	+1	1317	513	0.04	+1	1094	736	0.00	+1
R30	1213	617	0.03	+1	1008	822	0.05	+1	1207	623	0.05	+1	1076	754	0.10	0	966	864	0.04	+1
$w/t/l$	28/1/1				27/3/0				27/3/0				26/4/0				23/5/2			

Tablec13 Extreme points on the Pareto fronts for all proposed approach in the set R test instance

Test instances	MOEA/D			MOPSO			MOVPL			MOVPL-RP			MOVPL-RP-DO			MOVPL-RP-DO-AWA		
	z_1	z_2	z_3	z_1	z_2	z_3	z_1	z_2	z_3	z_1	z_2	z_3	z_1	z_2	z_3	z_1	z_2	z_3
R01	26.73	195.62	3	26.33	192.54	2	23.94	174.15	3	23.34	179.54	3	21.35	161.23	3	19.95	156.25	3
R02	30.05	221.15	2	29.36	215.85	3	30.51	224.69	3	28.22	217.08	2	25.25	184.23	3	22.94	171.17	3
R03	27.31	200.08	3	26.88	196.77	3	25.35	185	3	27.31	210.08	3	27.09	201.38	4	21.85	188.08	4
R04	39.72	295.54	3	37.58	279.08	3	36.35	269.62	4	33.61	258.54	3	32.08	236.77	3	30.55	234.58	4
R05	41.13	306.38	5	37.88	281.38	5	38.76	288.15	5	37.58	289.08	5	34.62	256.31	5	29.59	246.58	6
R06	41.96	312.77	5	41.64	310.31	5	39.76	295.85	5	36.95	284.23	5	39.14	301.08	5	31.31	259.92	6
R07	44.72	334	6	40.66	302.77	5	39.64	294.92	5	38.28	294.46	6	38.28	294.46	6	33.88	279.33	7
R08	42.14	314.15	6	45.94	343.38	6	41.45	308.85	6	39.38	302.92	6	37.99	292.23	6	34.54	282.83	7
R09	47.2	353.08	6	51.42	385.54	6	47.96	358.92	7	47.2	363.08	6	40.29	309.92	7	38.37	311.75	8
R10	49.57	371.31	7	49.57	371.31	7	45.1	336.92	8	48.08	369.85	7	42.12	321.21	8	37.27	310.58	9
R11	51.14	383.38	7	51.93	389.46	8	49.96	374.31	8	44.45	341.92	7	47.21	353.15	7	39.34	323.83	9
R12	62.6	471.54	8	64.07	482.85	8	57.22	430.15	8	56.25	432.69	8	53.81	403.92	9	48.91	410.58	10
R13	65.83	496.38	9	67.87	512.08	9	61.24	461.08	8	65.83	506.38	9	57.15	429.62	9	51.03	415.25	11
R14	74.46	562.77	9	66.13	498.69	9	73.35	554.23	10	68.91	530.08	9	58.91	443.15	10	55.57	453.08	12
R15	82.56	625.08	11	70.76	534.31	11	76.07	575.15	9	74.31	571.62	11	71.94	543.38	11	58.97	488.42	13
R16	79.15	598.85	11	82.84	627.23	10	73.02	551.69	11	73.02	561.69	11	69.95	528.08	11	61.36	511.33	13
R17	85.25	645.77	10	81.81	619.31	12	92.81	703.92	10	78.38	602.92	10	77.45	585.77	12	68.75	570.92	14
R18	92.25	699.62	12	93.68	710.62	11	85.1	644.62	12	82.24	632.62	12	84.38	639.08	14	71.51	593.92	15
R19	108.62	825.54	13	105.43	801	14	106.23	807.15	13	98.24	755.69	13	91.05	690.38	14	79.87	660.58	16
R20	123.6	940.77	13	115.05	875	15	112.19	853	12	122.65	943.46	13	113.15	860.38	14	95.08	785.33	17
R21	127.7	972.31	13	132.77	1011.3	13	134.8	1026.9	11	129.73	997.92	13	116.55	886.54	14	101.35	834.58	16
R22	160.75	1226.5	13	152.66	1164.3	16	153.81	1173.2	15	137.62	1058.6	13	127.22	968.62	15	115.65	951.75	18
R23	144.46	1101.2	14	146.81	1119.3	13	138.59	1056.1	16	137.42	1057.1	14	144.46	1101.2	17	117.45	971.75	19
R24	145.79	1111.5	15	146.99	1120.7	15	158.94	1212.6	16	137.43	1057.2	15	146.99	1120.7	15	119.5	965.83	18
R25	181.79	1388.4	17	159.72	1218.6	18	171.4	1308.5	17	151.92	1168.6	17	138.94	1058.8	17	129.85	1062.1	20
R26	155.67	1187.5	15	176.25	1345.8	15	151.81	1157.8	17	155.67	1197.5	15	156.95	1197.3	17	128.65	1071.1	21
R27	178.6	1363.8	17	168.09	1283	18	156.27	1192.1	15	157.58	1212.2	17	160.21	1222.4	20	131.32	1089.3	22

Table 13 (continued)

Test instances	MOEA/D			MOPSO			MOVPL			MOVPL-RP			MOVPL-RP-DO			MOVPL-RP-DO-AWA		
	z_1	z_2	z_3	z_1	z_2	z_3	z_1	z_2	z_3	z_1	z_2	z_3	z_1	z_2	z_3	z_1	z_2	z_3
R28	168.47	1285.9	19	160.51	1224.7	20	172.45	1316.5	21	157.85	1214.2	19	155.21	1183.9	20	132.65	1101.4	23
R29	187.63	1433.3	18	196.36	1500.5	21	183.27	1399.8	19	162.9	1253.1	18	168.72	1287.8	20	145.45	1202.1	23
R30	201.58	1540.6	16	200.11	1529.3	18	185.4	1416.2	16	161.85	1245	16	163.33	1246.4	19	147.14	1216.2	22

Table 14 Extreme points on the Pareto fronts for all proposed approach in the set RC test instance

Test instances	MOEA/D			MOPSO			MOVPL			MOVPL-RP			MOVPL-RP-DO			MOVPL-RP-DO-AWA		
	z_1	z_2	z_3	z_1	z_2	z_3	z_1	z_2	z_3	z_1	z_2	z_3	z_1	z_2	z_3	z_1	z_2	z_3
RC01	24.592	183.88	2	22.907	171.36	3	22.264	156.74	2	21.473	157.99	2	18.575	153.17	3	17.756	146.88	3
RC02	25.843	201.25	2	25.837	194.26	3	26.849	195.48	2	25.68	199.71	3	21.463	173.18	3	20.417	147.2	3
RC03	25.125	188.07	3	24.998	186.93	3	23.322	164.65	3	24.579	191.17	4	23.027	177.22	3	19.01	161.75	4
RC04	36.542	268.94	4	35.325	251.17	4	31.988	239.96	4	28.569	230.1	4	29.834	210.72	4	28.106	206.43	5
RC05	38.662	266.55	5	34.092	256.06	5	35.272	250.69	5	34.949	265.95	5	31.158	235.8	5	25.447	221.93	6
RC06	36.505	294	5	38.725	276.17	5	34.591	251.47	5	31.408	267.18	5	34.052	258.93	5	26.614	246.92	6
RC07	39.354	313.96	5	37.001	281.58	6	33.694	250.68	6	32.921	250.29	6	35.218	270.9	6	32.186	251.4	7
RC08	40.033	282.74	5	43.643	322.78	6	38.549	290.32	6	33.473	269.6	6	33.051	248.4	6	30.741	268.69	7
RC09	40.12	321.3	6	44.735	354.7	7	45.562	312.26	6	41.536	319.51	7	35.455	278.93	7	32.615	271.22	8
RC10	.596	330.46	7	44.117	334.18	8	40.59	306.6	7	41.83	321.77	7	38.75	305.15	8	32.798	276.42	9
RC11	47.56	360.38	7	46.737	342.73	8	46.463	355.59	7	38.227	321.41	7	42.961	314.31	8	34.619	278.5	9
RC12	56.34	405.52	8	56.382	453.88	9	52.07	382.84	9	50.625	367.79	10	48.429	347.37	10	45.486	381.84	11
RC13	56.614	421.93	8	61.083	476.23	9	56.341	414.97	9	57.93	455.75	9	53.721	399.54	10	44.396	357.12	11
RC14	69.992	495.24	9	56.872	453.81	10	64.548	520.98	10	60.641	477.07	9	55.965	407.7	10	52.236	430.43	12
RC15	71.002	593.82	9	64.392	486.22	10	69.224	540.64	10	69.108	520.17	9	64.027	478.18	10	51.304	420.04	12
RC16	75.193	556.93	10	74.556	545.69	11	62.797	474.46	11	66.448	483.06	11	63.655	475.27	11	52.77	444.86	13
RC17	76.725	607.02	11	73.629	582.15	12	85.385	647.61	11	74.461	530.57	12	65.833	521.33	12	62.563	496.7	14
RC18	87.638	650.64	11	88.996	625.34	12	79.143	547.92	11	74.838	550.38	12	72.567	575.17	12	64.359	516.71	14
RC19	101.02	709.96	12	100.16	760.95	13	91.358	742.58	12	90.381	695.24	11	81.035	593.73	13	67.89	614.34	15
RC20	112.48	809.06	12	101.24	805	14	102.09	742.11	13	107.93	801.94	13	100.7	782.95	14	80.818	706.8	16
RC21	113.65	836.18	13	124.8	950.63	14	117.28	975.58	14	121.95	868.19	14	100.23	780.15	15	89.188	709.4	17
RC22	146.28	1128.4	14	132.81	1036.2	15	146.12	1114.5	15	127.99	1005.7	16	117.04	862.07	16	105.24	885.13	18
RC23	135.79	991.11	13	135.07	962.6	14	117.8	992.71	14	126.43	1004.2	13	124.24	969.08	15	102.18	855.14	17
RC24	135.58	1022.5	15	139.64	1064.7	17	150.99	1030.7	16	129.18	993.72	15	138.17	1019.8	17	106.36	840.28	20
RC25	161.79	1180.1	15	143.75	1072.4	16	154.26	1230	15	144.32	993.32	15	122.27	910.54	17	118.16	987.74	19
RC26	136.99	1045	15	156.86	1278.5	17	133.59	1088.3	16	143.22	1101.7	16	133.41	1101.5	17	109.35	942.55	20
RC27	153.6	1227.5	16	149.6	1180.4	18	146.89	1060.9	17	133.94	1151.5	18	152.2	1063.5	18	116.87	969.51	21

Table 14 (continued)

Test instances	MOEA/D			MOPSO			MOVPL			MOVPL-RP			MOVPL-RP-DO			MOVPL-RP-DO-AWA		
	z_1	z_2	z_3	z_1	z_2	z_3	z_1	z_2	z_3	z_1	z_2	z_3	z_1	z_2	z_3	z_1	z_2	z_3
RC28	151.62	1105.9	16	136.43	1163.5	18	146.58	1198.1	17	148.38	1117.1	17	135.03	1018.2	18	118.06	1046.3	21
RC29	165.11	1361.6	18	168.87	1290.4	20	163.11	1301.8	19	153.13	1177.9	19	160.28	1171.9	20	125.09	1105.9	23
RC30	191.5	1432.8	17	180.1	1330.5	19	159.44	1217.9	18	147.28	1070.7	19	148.63	1121.7	19	126.54	1058.1	22

Table 15 Extreme points on the Pareto fronts for all proposed approach in the set C test instance

Test instances	MOEA/D			MOPSO			MOVPL			MOVPL-RP			MOVPL-RP-DO			MOVPL-RP-DO-AWA		
	z_1	z_2	z_3	z_1	z_2	z_3	z_1	z_2	z_3	z_1	z_2	z_3	z_1	z_2	z_3	z_1	z_2	z_3
C01	22.378	180.2	2	22.22	162.79	2	21.596	153.6	2	19.755	154.83	3	17.832	148.57	3	17.045	133.66	3
C02	23.776	187.16	2	23.253	186.49	3	25.506	179.84	3	23.626	183.73	3	20.175	164.52	3	18.783	139.84	3
C03	22.613	174.91	3	22.499	171.98	2	20.99	154.77	4	23.104	185.43	3	21.645	164.81	4	18.439	155.28	4
C04	34.715	242.05	4	32.499	243.63	4	29.749	220.76	3	27.997	225.5	5	26.851	189.65	5	27.544	189.92	5
C05	36.342	261.22	5	32.728	248.38	4	33.861	243.17	4	33.901	242.02	4	29.912	212.22	4	23.412	217.49	6
C06	34.315	285.18	5	37.951	262.37	4	32.17	241.41	4	29.523	240.46	4	33.371	243.39	4	25.283	222.23	6
C07	36.992	304.54	6	35.151	261.87	5	33.02	243.16	5	30.616	237.78	5	31.696	243.81	7	29.611	236.32	7
C08	36.03	274.26	6	40.152	316.33	6	37.392	267.09	6	32.469	261.51	6	30.407	233.49	6	29.818	255.26	8
C09	37.312	314.87	7	40.709	329.87	7	43.284	293.53	7	37.382	293.95	7	32.619	267.77	7	31.962	257.66	9
C10	44.6	317.25	7	41.47	324.15	7	36.937	288.2	6	40.575	315.33	7	36.038	299.05	7	31.486	257.07	9
C11	45.658	327.95	8	44.868	335.87	6	43.21	334.26	7	36.316	292.48	8	41.243	292.31	8	32.542	272.93	10
C12	51.269	393.36	9	52.435	426.64	8	47.384	352.21	8	45.563	356.75	9	45.039	333.48	10	41.393	343.66	11
C13	50.952	413.49	10	59.861	461.94	9	52.397	394.22	8	55.613	428.4	10	49.423	391.55	10	41.288	349.97	12
C14	63.693	460.57	9	54.597	422.04	8	61.966	489.72	10	58.822	434.13	10	52.047	383.24	10	49.624	404.6	12
C15	64.611	581.95	9	62.46	452.18	9	65.07	529.83	10	65.653	468.15	11	60.185	463.83	10	49.252	386.44	12
C16	72.937	534.65	10	68.592	496.58	11	60.285	441.24	10	59.803	458.9	10	61.745	451.51	11	51.187	413.72	13
C17	69.82	552.39	12	70.684	541.4	13	77.701	608.75	11	67.015	493.43	13	63.858	510.91	13	57.558	471.86	15
C18	82.379	618.11	13	87.216	600.33	12	73.603	520.53	10	72.593	500.84	13	71.115	523.4	13	61.141	470.2	15
C19	94.956	667.37	13	98.155	730.51	13	85.876	712.88	12	88.573	667.43	12	77.793	534.36	12	65.853	565.2	16
C20	107.98	792.88	13	95.169	772.8	14	91.884	712.43	12	99.297	785.9	14	96.675	704.66	15	74.353	636.12	17
C21	104.56	794.38	13	117.32	931.62	13	111.41	907.29	14	114.63	816.1	13	92.214	709.94	14	82.053	666.83	17
C22	140.43	1026.9	15	123.52	984.42	13	134.43	1003	14	116.47	965.46	13	114.7	844.83	16	102.08	814.32	18
C23	123.57	941.55	14	132.36	943.35	15	107.2	953	15	116.31	974.1	15	115.54	930.32	17	98.094	829.49	19
C24	126.09	930.52	14	131.26	979.49	14	138.91	999.8	16	124.02	914.23	15	127.12	938.24	18	95.72	798.26	19
C25	150.47	1097.5	15	130.81	975.87	14	146.55	1107	15	137.11	963.52	15	117.38	874.12	17	106.35	967.98	20
C26	132.88	1024.1	16	153.73	1214.6	14	120.23	1044.8	16	128.89	1068.6	19	124.07	991.37	19	102.79	857.72	20
C27	138.24	1166.1	17	134.64	1121.3	18	138.08	1039.7	16	124.57	1128.5	20	147.63	999.67	16	114.54	882.25	22

Table 15 (continued)

Test instances	MOEA/D			MOPSO			MOVPL			MOVPL-RP			MOVPL-RP-DO			MOVPL-RP-DO-AWA		
	z_1	z_2	z_3	z_1	z_2	z_3	z_1	z_2	z_3	z_1	z_2	z_3	z_1	z_2	z_3	z_1	z_2	z_3
C28	147.07	1039.5	17	122.79	1140.2	16	143.65	1090.2	17	133.54	1027.7	21	122.88	977.45	17	109.79	1015	22
C29	153.56	1279.9	18	162.11	1174.3	17	146.8	1275.7	16	139.34	1060.1	20	152.27	1078.2	18	117.58	1017.4	24
C30	181.93	1332.5	19	162.09	1210.8	18	151.47	1181.4	17	142.86	1038.6	17	141.2	1032	20	115.15	973.42	23

Acknowledgements This research is supported by the Computational Intelligence and Intelligent Optimization Research Group (CIIORG) of the Persian Gulf University (Grant Number PGU24-238641). It is also partly supported by the Czech Science Foundation (GACR), (Grant Number GA18-15530 S). We thank the editor and reviewers for their constructive feedback and valuable suggestions, which have significantly helped improve the quality of our article.

Funding Open access funding provided by Vienna University of Economics and Business (WU). 35 Persian Gulf University,PGU24-238641,Khodakaram Salimifard,Vysoká Škola Bánská—Technická Univerzita Ostrava,GA18- 15530 S,reza moghdani

Declarations

Ethical approval This article does not contain any studies with human participants or animals performed by any of the authors.

Conflict of interests The authors declare that there is no conflict of interest regarding the publication of this article.

References

Aleksandrov, M. (2025). Fairness and efficiency in social vehicle routing problems. *Transportation Research Procedia, 82*, 1994–2013.

Androutsopoulos, K. N., & Zografos, K. G. (2017). An integrated modelling approach for the bicriterion vehicle routing and scheduling problem with environmental considerations. *Transportation Research Part C: Emerging Technologies, 82*, 180–209. https://doi.org/10.1016/j.trc.2017.06.013

Audet, C., Bigeon, J., Cartier, D., Le Digabel, S., & Salomon, L. (2018). Performance indicators in multiobjective optimization. *Optimization Online 292* 2: 397-422.

Barth, M., & Boriboonsomsin, K. (2009). Energy and emissions impacts of a freeway-based dynamic ecodriving system. *Transportation Research Part D: Transport and Environment, 14*(6), 400–410. https://doi.org/10.1016/j.trd.2009.01.004

Bektaş, T., & Laporte, G. (2011). The pollution-routing problem. *Transportation Research Part B: Methodological, 45*(8), 1232–1250. https://doi.org/10.1016/j.trb.2011.02.004

Ben Ticha, H., Absi, N., Feillet, D., & Quilliot, A. (2018). Vehicle routing problems with road-network information: State of the art. *Networks, 72*(3), 393–406. https://doi.org/10.1002/net.21808

Bruglieri, M., Mancini, S., Pezzella, F., & Pisacane, O. (2016). A new mathematical programming model for the green vehicle routing problem. *Electronic Notes in Discrete Mathematics, 55*, 89–92. https://doi.org/10.1016/j.endm.2016.10.023

Bruglieri, M., Mancini, S., & Pisacane, O. (2019). The green vehicle routing problem with capacitated alternative fuel stations. *Computers & Operations Research, 112*, Article 104759. https://doi.org/10.1016/j.cor.2019.07.017

Comert, S. E., & Yazgan, H. R. (2023). A new approach based on hybrid ant colony optimization-artificial bee colony algorithm for multi-objective electric vehicle routing problems. *Engineering Applications of Artificial Intelligence, 123*, Article 106375.

Cui, H., Li, K., Jia, S., & Meng, Q. (2024). Dynamic collaborative truck-drone delivery with en-route synchronization and random requests. *Transportation Research Part E: Logistics and Transportation Review, 192*, Article 103802.

Dabia, S., Demir, E., & Woensel, T. V. (2017). An exact approach for a variant of the pollution-routing problem. *Transportation Science, 51*(2), 607–628. https://doi.org/10.1287/trsc.2015.0651

Dantzig, G. B., & Ramser, J. H. (1959). The truck dispatching problem. *Management Science, 6*(1), 80–91.
Das, I., & Dennis, J. E. (1998). Normal-boundary intersection: A new method for generating the Pareto surface in nonlinear multicriteria optimization problems. *SIAM Journal on Optimization, 8*(3), 631–657. https://doi.org/10.1137/S1052623496307510
Deb, K., & Jain, H. (2014). An evolutionary many-objective optimization algorithm using reference-point-based nondominated sorting approach, part I: Solving problems with box constraints. *IEEE Transactions on Evolutionary Computation, 18*(4), 577–601. https://doi.org/10.1109/TEVC.2013.2281535
Dehne, F., Omran, M. T., & Sack, J.-R. (2012). Shortest paths in time-dependent FIFO networks. *Algorithmica, 62*(1), 416–435. https://doi.org/10.1007/s00453-010-9461-6
Demir, E., Bektaş, T., & Laporte, G. (2012). An adaptive large neighborhood search heuristic for the pollution-routing problem. *European Journal of Operational Research, 223*(2), 346–359. https://doi.org/10.1016/j.ejor.2012.06.044
Demir, E., Bektaş, T., & Laporte, G. (2014a). The bi-objective pollution-routing problem. *European Journal of Operational Research, 232*(3), 464–478. https://doi.org/10.1016/j.ejor.2013.08.002
Demir, E., Bektaş, T., & Laporte, G. (2014b). A review of recent research on green road freight transportation. *European Journal of Operational Research, 237*(3), 775–793. https://doi.org/10.1016/j.ejor.2013.12.033
Donati, A. V., Montemanni, R., Casagrande, N., Rizzoli, A. E., & Gambardella, L. M. (2008). Time dependent vehicle routing problem with a multi ant colony system. *European Journal of Operational Research, 185*(3), 1174–1191. https://doi.org/10.1016/j.ejor.2006.06.047
Eglese, R., Maden, W., & Slater, A. (2006). A road timetableTM to aid vehicle routing and scheduling. *Computers & Operations Research, 33*(12), 3508–3519. https://doi.org/10.1016/j.cor.2005.03.029
Ehmke, J. F., Campbell, A. M., & Thomas, B. W. (2016a). Data-driven approaches for emissions-minimized paths in urban areas. *Computers & Operations Research, 67*, 34–47. https://doi.org/10.1016/j.cor.2015.08.013
Ehmke, J. F., Campbell, A. M., & Thomas, B. W. (2016b). Vehicle routing to minimize time-dependent emissions in urban areas. *European Journal of Operational Research, 251*(2), 478–494. https://doi.org/10.1016/j.ejor.2015.11.034
Elgharably, N., Easa, S., Nassef, A., & Damatty, A. E. (2022). Stochastic Multi-Objective Vehicle Routing Model in Green Environment With Customer Satisfaction. *IEEE Transactions on Intelligent Transportation Systems*. https://doi.org/10.1109/TITS.2022.3156685
Elshaer, R., & Awad, H. (2020). A taxonomic review of metaheuristic algorithms for solving the vehicle routing problem and its variants. *Computers & Industrial Engineering, 140*, Article 106242.
Eltoukhy, A. E., Hashim, H. A., Hussein, M., Khan, W. A., & Zayed, T. (2025). Sustainable vehicle route planning under uncertainty for modular integrated construction: Multi-trip time-dependent VRP with time windows and data analytics. *Annals of Operations Research*. https://doi.org/10.1007/s10479-024-06442-2
Emami, E., & Ramezani, M. (2024). Integrated operator and user-based rebalancing and recharging in dockless shared e-micromobility systems. *Communications in Transportation Research, 4*, Article 100155.
Erdoğan, S., & Miller-Hooks, E. (2012). A green vehicle routing problem. *Transportation Research Part E: Logistics and Transportation Review, 48*(1), 100–114. https://doi.org/10.1016/j.tre.2011.08.001
Fernández Gil, A., Lalla-Ruiz, E., Gómez Sánchez, M., & Castro, C. (2023). The cumulative vehicle routing problem with time windows: models and algorithm. *Annals Operations Research, 350*(1), 1–29.
Ferreira, K. M., de Queiroz, T. A., Munari, P., & Toledo, F. M. B. (2024). A variable neighborhood search for the green vehicle routing problem with two-dimensional loading constraints and split delivery. *European Journal of Operational Research, 316*(2), 597–616.
Figliozzi, M. A. (2011). The impacts of congestion on time-definitive urban freight distribution networks CO2 emission levels: Results from a case study in Portland, Oregon. *Transportation Research Part C: Emerging Technologies, 19*(5), 766–778. https://doi.org/10.1016/j.trc.2010.11.002
Fleischmann, B., Gietz, M., & Gnutzmann, S. (2004). Time-varying travel times in vehicle routing. *Transportation Science, 38*(2), 160–173. https://doi.org/10.1287/trsc.1030.0062
Franceschetti, A., Honhon, D., Van Woensel, T., Bektaş, T., & Laporte, G. (2013). The time-dependent pollution-routing problem. *Transportation Research Part B: Methodological, 56*, 265–293. https://doi.org/10.1016/j.trb.2013.08.008
Garside, A. K., Ahmad, R., & Muhtazaruddin, M. N. B. (2024). A recent review of solution approaches for Green Vehicle Routing Problem and its variants. *Operations Research Perspectives*. https://doi.org/10.1016/j.orp.2024.100303
Gendreau, M., Ghiani, G., & Guerriero, E. (2015). Time-dependent routing problems: A review. *Computers & Operations Research, 64, 189-197.* https://doi.org/10.1016/j.cor.2015.06.001
Ghosh, S., & Roy, S. K. (2023). Closed-loop multi-objective waste management through vehicle routing problem in neutrosophic hesitant fuzzy environment. *Applied Soft Computing, 148*, Article 110854.

Goli, A., Aazami, A., & Jabbarzadeh, A. (2018). Accelerated cuckoo optimization algorithm for capacitated vehicle routing problem in competitive conditions. *International Journal of Artificial Intelligence*, *16*(1), 88-112. http://www.ceser.in/ceserp/index.php/ijai/article/view/5444

Goodarzi, A. H., Jabbarzadeh, A., Fahimnia, B., & Paquet, M. (2024). Evaluating the sustainability and resilience of an intermodal transport network leveraging consolidation strategies. *Transportation Research Part E: Logistics and Transportation Review, 188*, Article 103616.

Grote, M., Williams, I., Preston, J., & Kemp, S. (2016). Including congestion effects in urban road traffic CO2 emissions modelling: Do local government authorities have the right options? *Transportation Research Part D: Transport and Environment, 43*, 95–106.

Hu, H., Zhang, Y., Wei, J., Zhan, Y., Zhang, X., Huang, S., Ma, G., Deng, Y., & Jiang, S. (2022). Alibaba vehicle routing algorithms enable rapid pick and delivery. *INFORMS Journal on Applied Analytics, 52*(1), 27–41.

Huang, Y., Zhao, L., Van Woensel, T., & Gross, J.-P. (2017). Time-dependent vehicle routing problem with path flexibility. *Transportation Research Part B: Methodological, 95*, 169–195. https://doi.org/10.1016/j.trb.2016.10.013

Ibarra-Rojas, O. J., & Silva-Soto, Y. (2021). Vehicle routing problem considering equity of demand satisfaction. *Optimization Letters, 15*(6), 2275–2297. https://doi.org/10.1007/s11590-021-01704-5

Ichoua, S., Gendreau, M., & Potvin, J.-Y. (2003). Vehicle dispatching with time-dependent travel times. *European Journal of Operational Research, 144*(2), 379–396. https://doi.org/10.1016/S0377-2217(02)00147-9

Jabali, O., Van Woensel, T., & de Kok, A. G. (2012). Analysis of travel times and CO2 emissions in time-dependent vehicle routing. *Production and Operations Management, 21*(6), 1060–1074. https://doi.org/10.1111/j.1937-5956.2012.01338.x

Jeong, J., Ghaddar, B., Zufferey, N., & Nathwani, J. (2024). Adaptive robust electric vehicle routing under energy consumption uncertainty. *Transportation Research Part C: Emerging Technologies, 160*, Article 104529.

Jozefowiez, N., Semet, F., & Talbi, E.-G. (2009). An evolutionary algorithm for the vehicle routing problem with route balancing. *European Journal of Operational Research, 195*(3), 761–769. https://doi.org/10.1016/j.ejor.2007.06.065

Kok, A. L., Hans, E. W., & Schutten, J. M. J. (2012). Vehicle routing under time-dependent travel times: The impact of congestion avoidance. *Computers & Operations Research, 39*(5), 910–918. https://doi.org/10.1016/j.cor.2011.05.027

Konstantakopoulos, G. D., Gayialis, S. P., & Kechagias, E. P. (2022). Vehicle routing problem and related algorithms for logistics distribution: A literature review and classification. *Operational Research, 22*(3), 2033–2062.

Kopfer, H. W., & Kopfer, H. (2013). Emissions Minimization Vehicle Routing Problem in Dependence of Different Vehicle Classes. In H.-J. Kreowski, B. Scholz-Reiter, & K.-D. Thoben, Springer *Dynamics in Logistics* Berlin, Heidelberg.

Kuo, Y. (2010). Using simulated annealing to minimize fuel consumption for the time-dependent vehicle routing problem. *Computers & Industrial Engineering, 59*(1), 157–165. https://doi.org/10.1016/j.cie.2010.03.012

Kwon, Y.-J., Choi, Y.-J., & Lee, D.-H. (2013). Heterogeneous fixed fleet vehicle routing considering carbon emission. *Transportation Research Part D: Transport and Environment, 23*, 81–89. https://doi.org/10.1016/j.trd.2013.04.001

Labuschagne, C., Brent, A. C., & van Erck, R. P. G. (2005). Assessing the sustainability performances of industries. *Journal of Cleaner Production, 13*(4), 373–385. https://doi.org/10.1016/j.jclepro.2003.10.007

Lacomme, P., Prins, C., Prodhon, C., & Ren, L. (2015). A multi-start split based path relinking (MSSPR) approach for the vehicle routing problem with route balancing. *Engineering Applications of Artificial Intelligence, 38*, 237–251. https://doi.org/10.1016/j.engappai.2014.10.024

Lee, S., Hong, D., Kim, J., Baek, D., & Chang, N. (2022). Congestion-aware multi-drone delivery routing framework. *IEEE Transactions on Vehicular Technology, 71*(9), 9384–9396.

Li, W., Zhang, Q., Huang, M., & Yu, Y. (2021, 22–24 May 2021). Multi-depot vehicle routing problem considering customer satisfaction. 2021 33rd Chinese Control and Decision Conference (CCDC),

Li, X. (2024). Multi-objective multi-compartment vehicle routing problem of fresh products with the promised latest delivery time. *Annals of Operations Research*. https://doi.org/10.1007/s10479-024-06254-4

Li, J.-Q., Borenstein, D., & Mirchandani, P. B. (2008). Truck scheduling for solid waste collection in the city of Porto Alegre, Brazil. *Omega (Westport), 36*(6), 1133–1149. https://doi.org/10.1016/j.omega.2006.04.007

Li, Y., Soleimani, H., & Zohal, M. (2019). An improved ant colony optimization algorithm for the multi-depot green vehicle routing problem with multiple objectives. *Journal of Cleaner Production, 227*, 1161–1172. https://doi.org/10.1016/j.jclepro.2019.03.185

Lin, C., Choy, K. L., Ho, G. T. S., Chung, S. H., & Lam, H. Y. (2014). Survey of green vehicle routing problem: Past and future trends. *Expert Systems with Applications, 41*(4, Part 1), 1118–1138. https://doi.org/10.1016/j.eswa.2013.07.107

Ma, Z., Jen, C. T., & Aazami, A. (2025). Time-Dependent Vehicle Routing Optimization Incorporating Pollution Reduction Using Hybrid Gray Wolf Optimizer and Neural Networks. *Sustainability 17*(11), 4829. https://doi.org/10.3390/su17114829

Maden, W., Eglese, R., & Black, D. (2010). Vehicle routing and scheduling with time-varying data: A case study. *Journal of the Operational Research Society, 61*(3), 515–522. https://doi.org/10.1057/jors.2009.116

Malandraki, C., & Daskin, M. S. (1992). Time dependent vehicle routing problems: Formulations, properties and heuristic algorithms. *Transportation Science, 26*(3), 185–200. https://doi.org/10.1287/trsc.26.3.185

Malandraki, C., & Dial, R. B. (1996). A restricted dynamic programming heuristic algorithm for the time dependent traveling salesman problem. *European Journal of Operational Research, 90*(1), 45–55.

Mancini, S. (2017). The hybrid vehicle routing problem. *Transportation Research Part C: Emerging Technologies, 78*, 1–12. https://doi.org/10.1016/j.trc.2017.02.004

Moghdani, R., & Salimifard, K. (2018). Volleyball premier league algorithm. *Applied Soft Computing, 64*, 161–185. https://doi.org/10.1016/j.asoc.2017.11.043

Moghdani, R., Salimifard, K., Demir, E., & Benyettou, A. (2020). Multi-objective volleyball premier league algorithm. *Knowledge-Based Systems, 196*, Article 105781. https://doi.org/10.1016/j.knosys.2020.105781

Moghdani, R., Salimifard, K., Demir, E., & Benyettou, A. (2021). The green vehicle routing problem: A systematic literature review. *Journal of Cleaner Production, 279*, Article 123691. https://doi.org/10.1016/j.jclepro.2020.123691

Moutaoukil, A., Neubert, G., & Derrouiche, R. (2014). A Comparison of Homogeneous and Heterogeneous Vehicle Fleet Size in Green Vehicle Routing Problem. In B. Grabot, B. Vallespir, S. Gomes, A. Bouras, & D. Kiritsis, *Advances in Production Management Systems. Innovative and Knowledge-Based Production Management in a Global-Local World* Berlin, Heidelberg.

Neggaz, N., Ewees, A. A., Elaziz, M. A., & Mafarja, M. (2020). Boosting salp swarm algorithm by sine cosine algorithm and disrupt operator for feature selection. *Expert Systems with Applications, 145*, Article 113103. https://doi.org/10.1016/j.eswa.2019.113103

Nekooghadirli, N., Gendreau, M., Potvin, J. Y., & Vidal, T. (2025). Workload equity in multiperiod vehicle routing problems. *International Transactions in Operational Research*. https://doi.org/10.1111/itor.70012

Pilati, F., & Tronconi, R. (2024). Multi-objective optimisation for sustainable few-to-many pickup and delivery vehicle routing problem. *International Journal of Production Research, 62*(9), 3146–3175.

Priyadarshi, R. (2024). Energy-efficient routing in wireless sensor networks: A meta-heuristic and artificial intelligence-based approach: A comprehensive review. *Archives of Computational Methods in Engineering, 31*(4), 2109–2137.

Purvis, B., Mao, Y., & Robinson, D. (2019). Three pillars of sustainability: In search of conceptual origins. *Sustainability Science, 14*(3), 681–695. https://doi.org/10.1007/s11625-018-0627-5

Qian, J., & Eglese, R. (2014). Finding least fuel emission paths in a network with time-varying speeds. *Networks, 63*(1), 96–106. https://doi.org/10.1002/net.21524

Qian, J., & Eglese, R. (2016). Fuel emissions optimization in vehicle routing problems with time-varying speeds. *European Journal of Operational Research, 248*(3), 840–848. https://doi.org/10.1016/j.ejor.2015.09.009

Qin, G., Tao, F., & Li, L. (2019). A vehicle routing optimization problem for cold chain logistics considering customer satisfaction and carbon emissions. *International Journal of Environmental Research and Public Health, 16*(4), Article 576.

Raeesi, R., & Zografos, K. G. (2019). The multi-objective steiner pollution-routing problem on congested urban road networks. *Transportation Research Part B: Methodological, 122*, 457–485. https://doi.org/10.1016/j.trb.2019.02.008

Rahiminia, S., Mehrabi, A., Jabbarzadeh, A., & Aghaee, M. P. (2025). A hybrid optimization approach for designing sustainable intermodal freight transport under mixed uncertainty. *Socio-Economic Planning Sciences, 98*, Article 102146.

Rajak, S., & P. P., & Dhanalakshmi, R. (2020). Multi-depot vehicle routing problem based on customer satisfaction. *International Journal of Services Technology and Management, 26*(2–3), 252–265.

Ramos, T. R. P., & Oliveira, R. C. (2011). Delimitation of service areas in reverse logistics networks with multiple depots. *Journal of the Operational Research Society, 62*(7), 1198–1210. https://doi.org/10.1057/jors.2010.83

Rastani, S., & Çatay, B. (2023). A large neighborhood search-based matheuristic for the load-dependent electric vehicle routing problem with time windows. *Annals of Operations Research, 324*(1), 1–33.

Revanna, J. K. C., & Al-Nakash, N. Y. B. (2023). Metaheuristic link prediction (MLP) using AI based ACO-GA optimization model for solving vehicle routing problem. *International Journal of Information Technology, 15*(7), 3425–3439.

Rojas-Saavedra, J. E., Álvarez-Martínez, D., & Escobar, J. W. (2023). Boosting sustainable development goals: a hybrid metaheuristic approach for the heterogeneous vehicle routing problem with three-dimensional packing constraints and fuel consumption. *Annals of Operations Research*. https://doi.org/10.1007/s10479-023-05533-w

Salehian, F., Tavakkoli-Moghaddam, R., & Norouzi, N. (2019). Solving a Vehicle Routing Problem Considering Customersق | ᒐ Satisfaction and Energy Consumption by a Bee Algorithm. *Quarterly Journal of Transportation Engineering, 11*(2), 299–311.

Solomon, M. M. (1987). Algorithms for the vehicle routing and scheduling problems with time window constraints. *Operations Research, 35*(2), 254–265. https://doi.org/10.1287/opre.35.2.254

Stamadianos, T., Taxidou, A., Marinaki, M., & Marinakis, Y. (2024). Swarm intelligence and nature inspired algorithms for solving vehicle routing problems: A survey. *Operational Research, 24*(3), 47.

Stølting Brodal, G., & Jacob, R. (2004). Time-dependent networks as models to achieve fast exact time-table queries. *Electronic Notes in Theoretical Computer Science, 92*, 3–15. https://doi.org/10.1016/j.entcs.2003.12.019

Tajik, N., Tavakkoli-Moghaddam, R., Vahdani, B., & Meysam Mousavi, S. (2014). A robust optimization approach for pollution routing problem with pickup and delivery under uncertainty. *Journal of Manufacturing Systems, 33*(2), 277–286. https://doi.org/10.1016/j.jmsy.2013.12.009

Tarhini, A., Danach, K., & Harfouche, A. (2022). Swarm intelligence-based hyper-heuristic for the vehicle routing problem with prioritized customers. *Annals of Operations Research, 308*(1), 1–22.

Vega-Mejía, C. A., Montoya-Torres, J. R., & Islam, S. M. (2019). Consideration of triple bottom line objectives for sustainability in the optimization of vehicle routing and loading operations: A systematic literature review. *Annals of Operations Research, 273*, 311–375.

Verbeeck, C., Vansteenwegen, P., & Aghezzaf, E.-H. (2017). The time-dependent orienteering problem with time windows: A fast ant colony system. *Annals of Operations Research, 254*, 481–505.

Wang, S., Yang, L., Yao, Y., Zhang, Q., & Shang, P. (2022). Equity-oriented vehicle routing optimization for catering distribution services with timeliness requirements. *IET Intelligent Transport Systems, 16*(2), 163–185.

Wang, W., Li, Y., Yan, H., Zhao, W., Zhao, Q., & Luo, K. (2025). A two-phase algorithm for the dynamic time-dependent green vehicle routing problem in decoration waste collection. *Expert Systems with Applications, 262*, Article 125570.

Woo, S., Choi, E. Y., Moura, S. J., & Borrelli, F. (2024). Saving energy with eco-friendly routing of an electric vehicle fleet. *Transportation Research Part E: Logistics and Transportation Review, 189*, Article 103644.

Worldbank. (2018). *Urban population (% of total population) - Iran, Islamic Rep*.

Xiao, J., Liu, X., Liu, T., Li, N., & Martinez-Sykora, A. (2024). The electric vehicle routing problem with synchronized mobile partial recharging and non-strict waiting strategy. *Annals of Operations Research*.https://doi.org/10.1007/s10479-024-06069-3

Yu, J. J. Q., & Li, V. O. K. (2015). A social spider algorithm for global optimization. *Applied Soft Computing, 30*, 614–627. https://doi.org/10.1016/j.asoc.2015.02.014

Yu, X.-P., Hu, Y.-S., & Wu, P. (2024). The consistent vehicle routing problem considering driver equity and flexible route consistency. *Computers & Industrial Engineering, 187*, Article 109803.

Zhang, P., Liu, Y., Yang, G., & Zhang, G. (2022). A multi-objective distributionally robust model for sustainable last mile relief network design problem. *Annals of Operations Research*, *309* (2) 1–42.

Zhang, J., Ge, Y.-E., Tang, C., & Zhong, M. (2024a). Optimising modular-autonomous-vehicle transit service employing coupling–decoupling operations plus skip-stop strategy. *Transportation Research Part E: Logistics and Transportation Review, 184*, Article 103450.

Zhang, S., Gajpal, Y., & Appadoo, S. (2018). A meta-heuristic for capacitated green vehicle routing problem. *Annals of Operations Research, 269*, 753–771.

Zhang, X., Zhang, Z., Liu, Y., Xu, Z., & Qu, X. (2024b). A review of machine learning approaches for electric vehicle energy consumption modelling in urban transportation. *Renewable Energy, 234*, Article 121243.

Authors and Affiliations

Reza Moghdani[1,2] · Khodakaram Salimifard[1] · Emrah Demir[3] · Sasan Barak[2,4] · Adel Aazami[5] · Seyed Ashkan Hosseini Shekarabi[6]

✉ Adel Aazami
adel.aazami@wu.ac.at

Reza Moghdani
reza.moghdani@gmail.com

Khodakaram Salimifard
salimifard@pgu.ac.ir

Emrah Demir
demire@cardiff.ac.uk

Sasan Barak
s.barak@soton.ac.uk

Seyed Ashkan Hosseini Shekarabi
s.hosseinishekarabi@ecu.edu.au

1 Computational Intelligence & Intelligent Optimization Research Group, Persian Gulf University, Bushehr, Iran

2 Faculty of Economics, VŠB Technical University of Ostrava, Ostrava 70200, Czech Republic

3 Business & Economics Artificial Intelligence Research Network, Cardiff Business School, Cardiff University, Cardiff CF10 3EU, UK

4 Department of Decision Analytics and Risk, Southampton Business School, University of Southampton, Southampton, UK

5 Institute for Transport and Logistics Management, Department of Global Business and Trade, Vienna University of Economics and Business, Vienna, Austria

6 School of Business and Law, Edith Cowan University, 270 Joondalup Drive, Joondalup, WA 6027, Australia